Calculation of extreme wind atlases using mesoscale modeling. Final report

Larsén, Xiaoli Guo; Badger, Jake

Publication date:
2012

Document Version
Publisher's PDF, also known as Version of record

Calculation of extreme wind atlases using mesoscale modeling

DTU Vindenergi
E Rapport 2016

Xiaoli Guo Larsén and Jake Badger

June 2012

DTU Wind Energy-E-0125

ISBN 978-87-93278-87-5

DTU Vindenergi
Institut for Vindenergi

Forfatter(e): Xiaoli Guo Larsén and Jake Badger
Titel: Calculation of extreme wind atlases using mesoscale modeling
Institut: Wind Energy Department, DTU

ISBN 978-87-93278-87-5

Kontrakt nr.:

Projektnr.:
PSO 10240

Sponsorship:
PSO ForskEL

Forside:

Sider: 38
Tabeller: [Tekst]
Referencer: 34

Danmarks Tekniske Universitet
DTU Vindenergi
Nils Koppels Allé
Bygning 403
2800 Kgs. Lyngby
Telefon

www.vindenergi.dtu.dk

Final Report for Project PSO-10240: Calculation of extreme wind atlases using mesoscale modeling

Xiaoli Guo Larsén and Jake Badger
Department of Wind Energy, Risø campus, DTU

June 30, 2012

Contents

Abstract

The objective of this project is to develop new methodologies for extreme wind atlases using mesoscale modeling. Three independent methodologies have been developed. All three methodologies are targeted at confronting and solving the problems and drawbacks in existing methods for extreme wind estimation regarding the use of modeled data (coarse resolution, limited representation of storms) and measurements (short period and technical issues).

The first methodology is called the selective dynamical downscaling method. For a chosen area, we identify the yearly strongest storms through global reanalysis data at each model grid point and run a mesoscale model, here the Weather Research and Forecasting (WRF) model, for all storms identified. Annual maximum winds and corresponding directions from each mesoscale grid point are then collected, post-processed and used in Gumbel distribution to obtain the 50-year wind.

The second methodology is called the statistical-dynamical downscaling method. For a chosen area, the geostrophic winds at a representative grid point from the global reanalysis data are used to obtain the annual maximum winds in 12 sectors for a period of 30 years. This results in 360 extreme geostrophic winds. Each of the 360 winds is used as a stationary forcing in a mesoscale model, here KAMM. For each mesoscale grid point the annual maximum winds are post-processed and used to a Gumbel fit to obtain the 50-year wind.

For the above two methods, the post-processing is an essential part. It calculates the speedup effects using a linear computation model (LINCOM) and corrects the winds from the mesoscale modeling to a standard condition, i.e. 10 m above a homogeneous surface with a roughness length 5 cm. Winds of the standard condition can then be put into a microscale model to resolve the local terrain and roughness effects around particular turbine sites. By converting both the measured and modeled winds to the same surface conditions through the post-processing procedure, it becomes possible to validate the measurements more reasonably.

The third method is called the spectral correction method. It is targeted at improving the general smoothing effect of mesoscale models for extreme wind application. Through wind time series of one year or more, or a spectral model if there are no measurements, we can add the wind variability to the mesoscale modeled time series, thus obtaining improved extreme wind estimation.

The first method has been applied to three areas with different degrees of terrain complexity, Denmark (flat), Gulf of Suez (medium complex) and Navara region in Spain (highly complex), and to places with different extreme wind mechanisms (the synoptic lows and the channeling winds). The second method has been applied to Denmark and Gulf of Suez. The two methods give quite consistent extreme wind atlases which agree well in general with the measurements from several sites; the first method has given better estimates for Gulf of Suez. The first method is more cost effective for larger areas. The third method

can generally be applied to any mesoscale modeled wind time series.

Even though the extreme wind atlases obtained with the new methodologies are quite satisfactory for non-complex terrains, challenges remain in (1) very complex terrains, e.g. mountains with steep cliffs, (2) coastal areas where land and water transit, (3) offshore where the unique wave dynamics during storm conditions have not been taken into account in the atmospheric modeling of the current methods.

1 Preface

This is the final report of the project PSO-10240 "Calculation of extreme wind atlases using mesoscale modeling". The overall objective is to improve the estimation of extreme winds by developing and applying new methodologies to confront the many weaknesses in the current methodologies as explained in Section 2. The focus has been put on developing a number of new methodologies through numerical modeling and statistical modeling.

The project proceeded as planed with additional findings. Two independent methods have been developed side by side, with one being focused on individual storm episodes that affect a particular area (the selective dynamical downscaling method, [1]) and one being focused on the extreme wind climate classified through the global data (the statistical-dynamical downscaling method)(Sections 6 and 7). The Weather Research and Forecasting (WRF) model was chosen for the storm simulations while both WRF and the Karlsruhe Atmospheric Mesoscale Model (KAMM) were planned for the extreme wind class simulation. For the selective dynamical method (Sel. Dyn. method), the WRF model is used in the forecast mode. For the statistical-dynamical downscaling method (Sta. Dyn. method), the WRF and KAMM models are used for the ideal case mode, which means the model is run with a static mean profile. After the start of the project, it was soon found out that for the ideal conditions, WRF is having trouble with the boundary conditions. Within the development of the statistical-dynamical downscaling method, the focus has then been put to the use of KAMM instead, with WRF as reference. The smoothing issues with numerical modeling, here mesoscale modeling in particular, underestimates the extreme wind substantially and it has to be taken into account. A statistical approach through spectral analysis is therefore developed to handle this general issue (Section 8, [2]). Almost all methods, the existing and the currently developed, are questioned about their reliability regarding the long term representativity due to limited number of years of data available, including modeled data. Statistical studies have been taken to investigate the issues related (Section 11, [3]).

The two dynamical down-scaling methodologies and the statistical downscaling approach have their own strength and drawbacks. The selective dynamical downscaling method is accurate but rather costly compared to the other two methods. It is mostly cost-efficient for a quite large areas. The statistical-dynamical downscaling method is computationally much cheaper. The statistical approach using the spectral correction is fast and cheap; it can be applied on top of existing modeled outputs.

It has always been a challenge to link the mesoscale and microscale modeling. There are many types of microscale models, here we put our focus on the linear model LINCOM which has been widely used within Wind Energy applications. This introduces another innovative approach within this project: the post-processing procedure that

handles the extreme wind outputs from the mesoscale modeling ([4]). Through the post-processing the mesoscale extreme winds are ready to be used as input for the microscale modeling, here through LINCOM.

The methods developed can be of general use. In principle, it can be applied both to flat terrains or complex terrains. Initially we had Denmark as the target. Denmark is a special place where the terrain is very simple and the methods have given satisfactory results in general in comparison with measurements. Even for the medium complex terrain in the Gulf of Suez, this method also worked quite satisfactorily, according to the measurements along the channel.

However, there are two situations where the extreme wind estimation remains high uncertainty: one is offshore and one is very complex terrain. For offshore, there misses a coupling of wave dynamics in the current mesoscale atmospheric modeling. The wave field interacts with the atmospheric flow movement and is directly related to the wind field. However, coupling the wave dynamics to the atmospheric modeling is not a trivial task, especially during storm conditions, and it is not possible to be realized within the framework of the current project. With the help of EU Safewind project, we have got the access to the data in a very complex terrain, the Navara region in Spain and therefore got the opportunity to test the method in such a challenging situation. A number of different and difficult situations appeared, in comparison with the simple and medium complex terrain. However, the crux is not caused by the methodology we developed here but by the limitation of the tools to handle the the more challenging match between modeling of different scales, namely the meso and micro scales in complex terrains. The linear microscale model becomes less useful in such complex terrain.

At the end of the project, we reached all milestones:

1. Mesoscale extreme wind atlases for Denmark and Gulf of Suez

2. The mesoscale modeling derived extreme winds for the selected regions can be used as input to WEng and extreme winds for particular wind farm sites can thus be obtained.

3. This final report

The whole work flow from global data to site use has been tested through a number of commercial applications and it is found to be very straightforward to apply and the results for the Danish sites (non-offshore) are satisfactory.

The work has been presented at quite a number of conferences and workshops, in the format of scientific and technical proceedings, oral and poster presentations. Two journal papers are published and two more are under construction. The complete list of the dissemination is given in Section 13.

In particular, the selective dynamical downscaling method has been published in the journal paper Larsén et al. 2012a [1]. The statistical correction method has been published in the journal paper Larsén et al. 2012b [2]. The statistical dynamical downscaling method has been published in a conference poster and abstract (Badger and Larsén 2012) and the details are documented in this report. Analysis on the

statistical uncertainties related to the fitting functions for the extreme winds is documented in the manuscript Larsén et al. 2012c.

Please find the major results related to the milestones:

1. The selective dynamical downscaling method: Figure 17, 24 and 34, Table 5 and 14.

2. The statistical-dynamical downscaling method: Figure 29b and Figure 31b.

3. Comparison of the results from the two methods: Table 12 and 13.

2 Objective and Background

This project is aimed at developing new methodologies to improve the estimate the extreme wind for wind turbine sitting.

The new methodologies are made to confront the existing difficulties in estimating the extreme winds using the conventional methods caused by

- limitations in measurements,
- limitations in mathematical models,
- limitations in the global and regional climate modeling and
- limitations in our ability of using modeled data to particular sites.

These are discussed in details in the following sections 2.1 to 2.4.

2.1 Using measurements

Long term measurements, on the order of 10 years, are needed to make a reliable estimation of the normally required design criteria of the 50-year return wind U_{50}. For an optimal situation, wind farm operators can have several years measurements; for many cases, they have only data for one year or two. High uncertainty is involved if the calculation is based on such a short time series (see detailed arguments in Section 11). Even when the long term measurements are available, the consistency in measuring technique, instrumentation, exact locations are often difficult to keep, not to mention the high technical difficulties of measuring during stormy forces. It is not rare that the measurements go wrong when the mast or the instrument is hit by the storm.

2.2 Using mathematical approaches

Mathematical approaches using the Monte Carlo type simulation have been considered by many (e.g. [5], [6], [7]). The benefit of using this approach is that one only needs a short time series (one year or a few years) to obtain some wind statistics and build a new time series of hundreds and even thousands of years that carry the same wind statistics. This of course also implies a serious flaw of this approach where long term variability is missing. The long term variability is very important in the extreme wind distribution and therefore the estimation of the T-year return wind; this is discussed more in details in Section 11.

2.3 Using global climate model data

The long term variability is expected to be well-presented by the global and regional climate models. The climatological data are therefore have been investigated and used for extreme wind estimations. Atmospheric reanalysis projects, such as those carried out by National Centers for Environment Prediction/National Center for Atmospheric Research (NCEP/NCAR) ([8]) and European Center for Medium range Weather Forecasting (ECMWF), use a large volume of measurements available through a sophisticated data assimilation system and thus

provide us with decades long and physics based data sets over the globe. The above mentioned reanalysis data are normally of spatial resolution of about 200 km or coarser and temporal resolution of 6 hours. It is not immediately clear how the coarse resolution data can be used for particular wind turbines since a fine resolution is essential for extreme wind conditions. Frank et al. ([9]) started applying the NCEP/NCAR reanalysis data for an extreme wind atlas over Denmark and found it was severely underestimated. Larsén and Mann ([10]) and Larsén et al. [11] analyzed the behavior of the NCEP/NCAR and ECMWF data for this purpose and concluded that a further downscaling approach is needed when applying the global data for site use.

Larsén and Mann [12] developed a theoretical and an empirical model to correct the coarse temporal resolution of the reanalysis data. The theoretical model is based on an assumption of Gaussian distribution of the wind speed, thus the mean annual wind maxima, and accordingly the 50-year wind, can be corrected from 6 hours to 10 min. The empirical model allows correction for wind from different sectors.

This can only partly cope with the resolution issue. In [9] and [10], the reanalysis data are linked to a microscale model LINCOM (Linear Computation Model) as embedded in the software WAsP Engineering (WEng), in order to resolve some of the spatial variability around the turbine sites. Instead of the surface winds, the geostrophic winds at sea level (G) are calculated from the pressure and temperature fields. G is then "extrapolated" to 10 m high, over a homogeneous surface with a roughness length of 5 cm, through the geostrophic drag law ([13]). The extrapolated winds are now of "standard conditions" and they can be put into the microscale model as in WEng.

[10] found that, this method using global data together with the correction for temporal resolution and downscaling using WEng works not too bad for places like Denmark where the extreme winds are predominately due to synoptic weather phenomenon, although including mesoscale variability will improve the estimates. For places where the extreme winds are of mesoscale phenomena, the estimation of the extreme winds has large uncertainty, as suggested by the comparisons with measurements.

It seems to suggest that if these mesoscale phenomena can be resolved, then we are safer - it is quite natural to assume a regional climate model (section 2.4) can do the job.

2.4 Using regional climate model data

Considering the ability of modeling mesoscale variability by the regional models, many investigators have used outputs from various regional climate models (RCMs).

Many RCM run-based studies have focused on general statistics of storms and strong winds, e.g. [14] and [15], or modeling of single storms, e.g. [16]. What these studies provide are quite different from what are needed for estimating the extreme wind for particular site

application. Some use the RCM outputs directly to calculate the 50-year wind, e.g. [17], [18], [19] and [20]. It is acceptable to use the model output this way for studies of climate change and trend, but the results should not be used directly as site conditions of wind farm. It is because the mesoscale modeling is normally accompanied with temporal and spatial smoothing issue embedded in the model setups. [2] analyzed outputs of a horizontal resolution from 10 km to 50 km from three well-used mesoscale models and demonstrated that, due to the smoothing effect of the mesoscale models, the zero- and second-order moments in the wind speed spectra are severely underestimated, which was shown to lead to significantly underestimated extreme winds.

There is another problem with some of the RCMs. After the model initiation, the models are only constrained by the boundary conditions, which sometimes results in storms that do not follow the same track as in the large scale data ([11]).

Often, it is computationally expensive to run the RCMs over a relatively large area at a fine resolution of 10 km.

3 Project structure

Methodologies are developed pointing at the problems discussed in the previous section. The two dynamical downscaling methods, the selective dynamical method and the statistical-dynamical method, have been developed simultaneously and they are introduced in Sections 6 and 7, respectively. The third method, the statistical model, for correcting the smoothing effect of the mesoscale modeling is described in Section 8.

Before the introduction of the methodologies, the data from models and observations are briefly introduced in Section 4 and the study area and sites are described in Section 5.

The studies have been done to three areas:

- Denmark, simple terrain, extreme winds are synoptical depressions.
- Gulf of Suez, medium complex terrain with mountain and channel, extreme winds are synoptical depression and channeling winds related to synoptical pressure gradient.
- Narara region, very complex terrain with mountains and valleys, extreme winds are forced by synoptical system combined with local terrain effects.

The results and detailed discussions are given in Section 9.

The findings from the project have contributed to a number of publications. More updated findings are described and discussed in this report only, including the sensitivity of the results on the use of which height of the winds (Section 9.1.1), the dependence of results on the year-to-year variation of storm (Section 9.1.1), the inclusion of the new cases in the latest year and their impact on the existing results, the spectral correction method applied to NRA data and complex terrains and many other issues in the complex terrains (Section 10).

4 Data

4.1 Data from global models

Two global model data are used here in this project. One is the NCEP/NCAR reanalysis (NRA) data and the other one is the NCEP final analysis (FNL) data.

The NRA-1 data are available from 1948. However there have been major changes in the operating systems. One of them is the data assimilation procedure due to more measurements become available through time, especially the upper air and satellite data. The period 1979 - present is self-consistent in this sense and it is therefore used here. The data are saved every 6 hours, with a spatial resolution about 2 degrees on Gaussian grids but 2.5 degrees for diagnostic variables.

The NCEP-DOE Reanalysis 2 (corresponding to NRA-2 data) is an improved version of the NCEP renalaysis 1 (corresponding to NRA-1 data) model that fixed errors and updated parameterizations of the physical processes ([21]).

The FNL data are available from 1999. The temporal resolution is also 6 hourly but the horizontal spatial resolution is 1 degree. When used as the boundary conditions for modeling the storms, this fine spatial resolution provides better storm structure at the initial condition, compared to the NRA data.

In Section 7, the NRA-2 data are used to obtain extreme wind classes which are later used as the initial and boundary conditions for the mesoscale KAMM model.

The NRA data are also used for storm identification in Section 6.1.

As shown in Section 6, the FNL data are used as the initial and boundary conditions for the WRF runs for the selective dynamical downscaling method.

4.2 Data from mesoscale modeling

The data from mesoscale modeling in this project are of three types.

The first is the outputs from RCMs where the spectral correction is needed in order to estimate the extreme winds (Section 8). Data from three RCMs were used in [1] to demonstrate the spatial smoothing effect of mesoscale modeling. One of the three RCMs is HIRHAM5 which combines the dynamical core of HIRLAM and physical parameterization schemes of the global model ECHAM5 (details can be found in [22]). HIRHAM has been forced by two global data: ERA-40 and ECHAM5. The spatial horizontal resolution is 25 km. The second of the three model is REMO from Max Plank Institute in Hamburg, Germany. It was forced by ERA-15 for 1979-93 and by ECMWF analysis data for 1994-2003. The spatial resolution is 50 km and 10 km. The third model is the WRF model, driven by NCEP reanalysis II. The horizontal resolution is 45 km and 15 km. The temporal resolution of all model outputs are hourly.

The second data is from the mesoscale modeling using KAMM for extreme wind classes (Section 7). The outputs are extreme wind classes

satisfying certain background large scale wind and thermal conditions throughout the atmospheric layers. The embedded temporal resolution is as the forcing, i.e. 6 hours. The spatial resolution has been set to 5 km in our studies.

The third data is from the WRF simulation for storm episodes. These are time series of a series of variables throughout the atmospheric layers during the storms. The temporal resolution of the output is 10 minutes and the spatial resolution is 5 km for the simple terrain case in Denmark, 3 km for the channel and mountainous terrains in the Gulf of Suez and 2 km for the complex mountainous terrains in the Navara region in Spain.

4.3 Measurements used for data validation

Measurements from the three areas, Denmark, Gulf of Suez and Navara region, are used.

Data for the Denmark case include also a couple of sites from Germany (FINO 1) and Sweden. Here, meteorological parameters (including wind speed, direction, temperature, pressure) at several heights ranging from 3 m to 100 m are available. The data are 10 min averages. Details of the locations of the site, measuring height and data coverage can be found in [1] (their Table II and Figure 3). Here several sites provide quite long time series that can be used to estimate the 50-year return wind.

Data for the Gulf of Suez case are mostly available at one level of 24.5 m. Measurements at 47.5 m are available at some sites for a short period. Measurements are mostly wind speed and direction. The data are also 10 min averages. Detailed information can also be found in [1] (their Table II and Figure 3).

Data from the Navara region are standard meteorological measurements from auto-stations from December 2003 to November 2010, 7 years. They are at 10 m height on hourly basis. The distribution of the sites in this area is shown in Fig. 1 ([23]). The analysis has been done to a number of sites, as listed in Table 14, where RIX of these sites were obtained from WAsP ([23]). In WAsP or WEng, the complexity of the terrain is described in terms of the ruggedness index RIX. In WAsP, it is calculated for each of a number of radii originating at the site. A flat site has a RIX of 0%. A complex steep site with an index of for instance 30% means that about 30% of the terrain is steeper than the critical slope. According to the RIX numbers, these sites are a mix of complex and simple terrains. The information about the coordinates of the sites, altitude and height of the sensor can be found in Table 1 in [24].

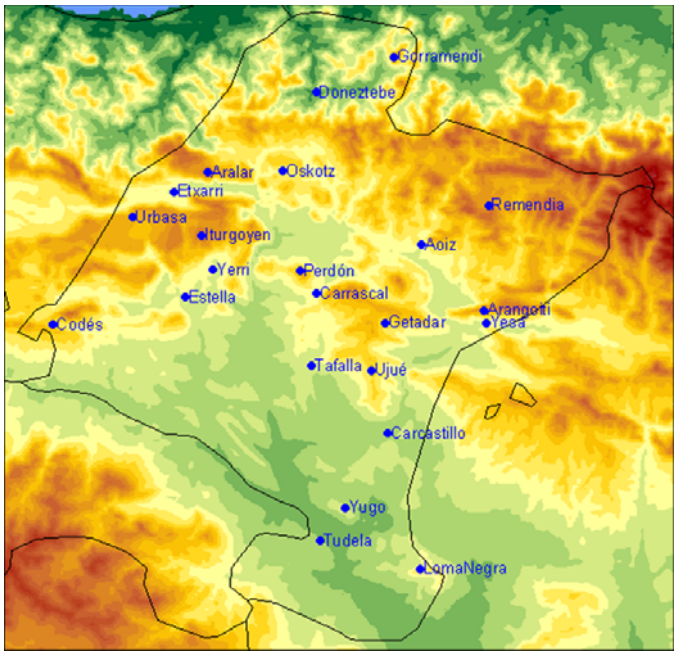

Figure 1: Met stations in the Navara region.

5 Study areas and sites

Among the three areas we studied here, Denmark represents a rather flat area with simple terrains. An elevation map of this area can be found in figure 3a and c in [1]. Fig. 2 shows the background roughness length as used in the WRF model over the area.

The Gulf of Suez is a relatively complex terrain area, with mountains up to about 2500 m and a channel. The topography of this area is plotted as elevation in figure 3b and d in [1]. Fig. 3 shows the background roughness length over the area as used in the WRF model.

The Navara region corresponds to a challengingly complex terrain with large mountains. Fig. 4 shows the high resolution terrain elevation and background roughness length in this area. A bigger area with the topography shown at a resolution of 18 km can be seen in Fig. 6c. Detailed description of the displacement of mountains and valleys in this area can be found in [24].

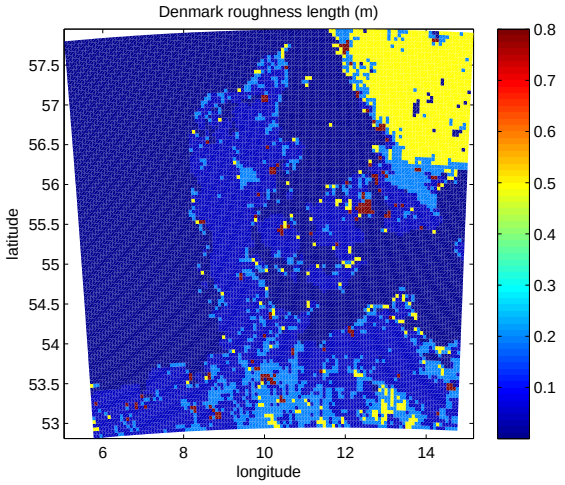

Figure 2: The roughness length for the Denmark case.

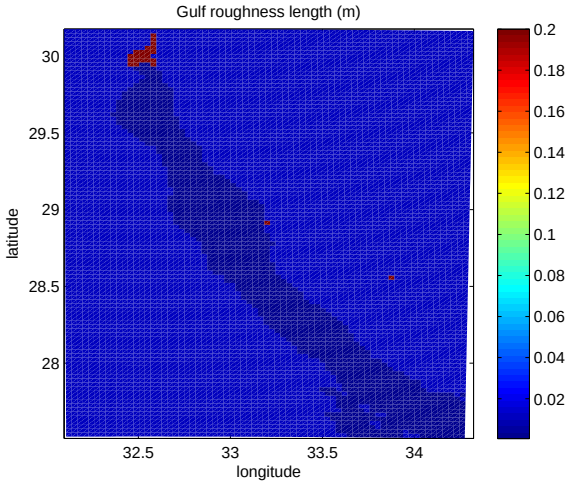

Figure 3: The roughness length for the Gulf of Suez case.

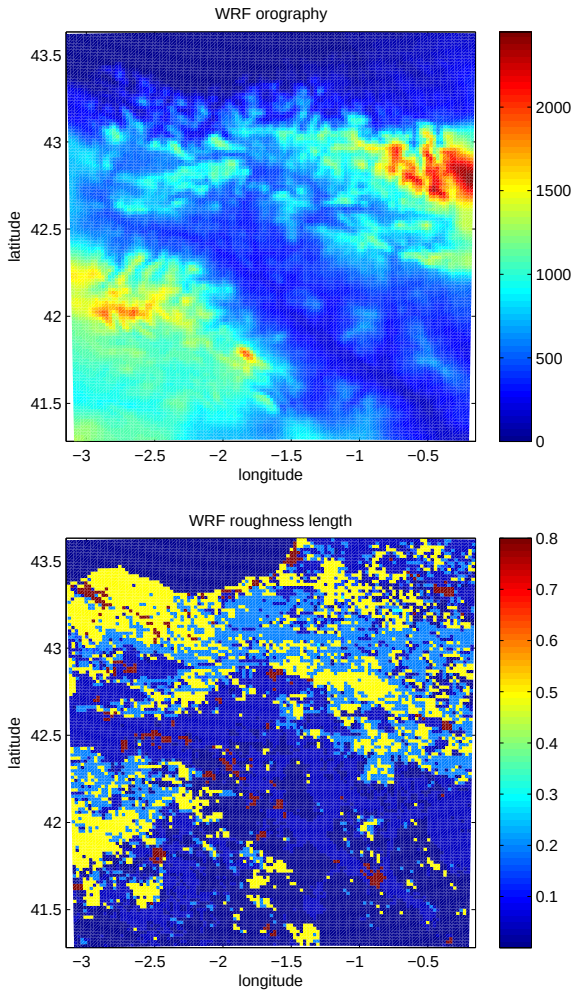

Figure 4: The elevation and roughness length for the Navara region.

6 The selective dynamical downscaling method

The phrase "selective" refers to the selection of the annual strongest wind episodes. There are three major steps in applying this method and they are briefly described in Sections 6.1 to 6.3. For the detailed description of this method, please refer to [1].

6.1 Identifying the storms

The NCEP/NCAR reanalysis (NRA) data are used to identify the storm episodes in the climate record. The period 1999 - present is chosen instead of the entire third era of NRA, namely 1979 - present, because the NCEP Final Analysis (FNL) data are used as the boundary and initial forcing of the Weather Forecasting and Research (WRF) modeling and the FNL data are only available since 1999. More details about the NRA and FNL data have been given in Section 4.1. In short, it is economical to use the NRA data to identify storms because of its relatively coarser resolution - the data files are of smaller sizes and easier to handle. It is also practical because all existing free global reanalysis/analysis data are of 6 hour resolution, data with finer horizontal resolution than the NRA data will still face similar issues of the size and duration of the storms being identified.

Two parameters are used for the identification: the wind speed at 10 m u_{10m} and the geostrophic wind at sea level G. Reanalysis pressure and temperature from 5 grid points, with positions (i,j), $(i-1,j)$, $(i+1,j)$, $(i,j-1)$ and $(i,j+1)$, were used to calculate the components of G, u_g and v_g, using the mean sea level pressure differences $\Delta P_{0,j}$ over $2\Delta\phi$ and $\Delta P_{0,i}$ over $2\Delta\lambda$:

$$u_g = -\frac{1}{f\rho}\frac{\Delta P_{0,j}}{2r\Delta\phi}, \quad v_g = \frac{1}{f\rho}\frac{\Delta P_{0,i}}{2r\Delta\lambda\ \cos\phi} \tag{1}$$

where r is the Earth radius and ρ is the air density. The geostrophic wind speed is $G = (u_g^2 + v_g^2)^{\frac{1}{2}}$. The latitude difference $\Delta\phi = \phi_{j+1} - \phi_j$ and longitude difference $\Delta\lambda = \lambda_{i+1} - \lambda_i$ are in radians. The air density is calculated through $\rho = P_{0,ij}/(RT_{0,ij})$, where R is the gas constant for dry air, $P_{0,ij}$ and $T_{0,ij}$ are the pressure and temperature at mean sea level at grid (i,j).

As an example, the NRA grid points for the Navara region are shown in Fig. 5. For each point, the dates when the yearly strongest G and yearly strongest u_{10m} occur, which are not always the same, are identified. For the Navara region, during 1999 - 2011, this results in 9 (grid points) $\times$ 13 (number of years in total) $\times$ 2 (for G and u_{10m}) time stamps. Some of these time stamps belong to the same storm. All together, for 1999 - 2011, there are 58 storm episodes for the Navara region and 63 storms for Denmark. For 1999 - 2010, there are 57 storms for Gulf of Suez area.

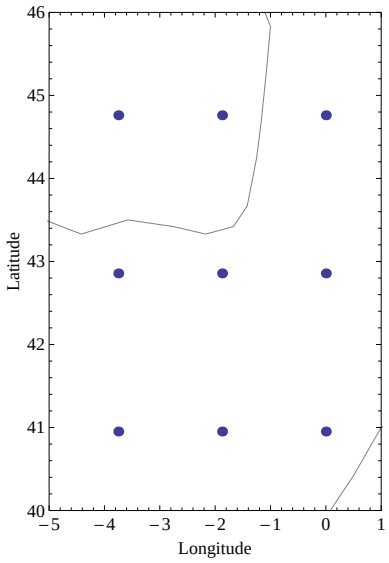

Figure 5: Domain with coastlines and the grid points of NRA data for storm identification. Navara region in Spain. Please refer to [1] for similar maps for Denmark and Gulf of Suez (their Fig. 2). See the location of the three domains in larger domains in Figure 6.

6.2 Simulation of the storm episodes

For the two main research domains, Denmark and Gulf of Suez, the Advanced Research WRF (ARW) core version 3.1 was used for the mesoscale modeling. Later in the project, the Navara region became our candidate for its complex terrain and by then we have the chance to use a newer version of WRF version 3.2.1 to simulate all storms.

We use the FNL data as the boundary layer forcing.

The individual storm events in the selected domains do not exceed more than 3 days. The simulation length is thus limited to 2-3 days according to the identified dates.

The half degree NCEP Reynolds Optimally interpolated sea surface temperature (SST) data sets are used. They are available since 2001. The simulations from 1999 to 2001 March are done with no SST input.

Different physics options have been tested through a number of case studies. The final choices include:

- Monin-Obukhov scheme for surface layer physics
- Lin et al. microphysics scheme
- Kain-Fritsch cumulus parameterization
- 6th order numerical diffusion with factors 0.06, 0.08 and 0.1 for the three domains
- positive advection of moisture and scalars
- the Yonsei University Planetary Boundary Layer (YU PBL) scheme
- hurricane option

We used 3 nested domains. Due to the terrain complexity of different degrees, the horizontal grid spacing is set as 45 - 15 - 5 km for Denmark, 27 - 9 - 3 km for Gulf of Suez and 18 - 6 - 2 km for the Navara region for the WRF domain I, II and III. For Denmark and Gulf of Suez, there are 37 levels in all domains. For the Navara region we used 41 vertical levels. We used one-way nesting technique. The outputs are saved every 10 min. The WRF domains for Denmark and Gulf of Suez are given in [1] (their Figure 3). The domains are plotted here as topography in Figure 6.

6.3 The post-processing procedure

The post-processing developed here is to prepare the mesoscale modeled winds for further downscaling using microscale models. It has always been a challenge how to link the mesoscale and microscale models.

The work was initiated by [4] and it uses the concept of WAsP and WEng to correct the effects from topography, roughness and roughness change in the upwind fetches. This process is called within this project as "generalization".

For each of the storm episodes, the application of the generalization is done. Figure 7 shows the examples of the maps of the correction factor for the orographic effect (δh) for winds from the west sector. The four subplots correspond to 10 m, 15 m, 52 m and 105 m, respectively. Similarly, Figure 8 shows maps of the correction factor for the roughness change (δr) at the four levels for the west sector. The effective roughness, z_{0E}, for the westerly wind is plotted in Figure 9. Unlike δr and δh, z_{0E} is not dependent on height. The details including the algorithms for the post-processing can be found in e.g. [1], [4], [25] and [26].

With the input of the roughness length (z_0) and elevation (h), the LINCOM program outputs the correction factors in such a way that the particular algorithm for correcting the two effects becomes:

$$u_z = u \cdot \delta r / \delta h, \tag{2}$$

where u_z represents the wind free of the orographical and roughness change effects. Thus, values of δr and δh close to 1 mean small correction. From Figures 7 and 8, it seems that δr contributes more to the total correction factor and it is much more significantly dependent on height compared to δh.

In order to obtain the winds of standard conditions, G needs to be calculated through

$$G = \frac{u_*}{\kappa}\sqrt{\left(\ln\frac{u_*}{f z_0} - A\right)^2 + B^2}, \tag{3}$$

where f is the Coriolis parameter, A and B are dimensionless parameters set to $A = 1.8$ and $B = 4.5$ according to [27]. For u_z, the corresponding roughness length is z_{0E}. We need input of the friction

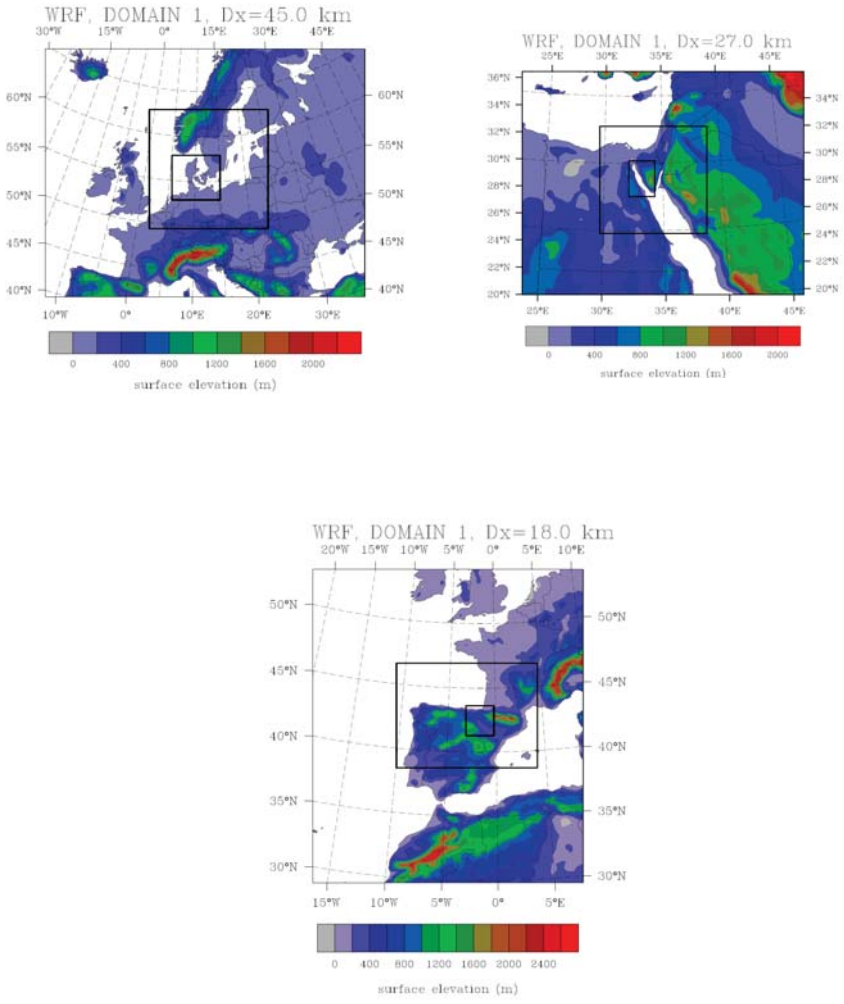

Figure 6: Three model domains of the WRF modeling shown as topography for Denmark (upper left), Gulf of Suez (upper right) and the Navara region (below).

velocity u_*, which, given the wind direction, could be calculated for the corresponding sector using the logarithmic wind law:

$$u_* = \frac{\kappa u_z}{\ln(z/z_{0E})}, \tag{4}$$

where $\kappa = 0.4$ is the von Kármán constant. In both Eq.s (3) and 4, neutral stability is assumed, which is reasonable for the extreme wind conditions studied here.

The core of the generalization is that G remains the same for the actual conditions and for the standard conditions. Now with the new roughness length, here $z_0 = 0.05$ m for a particular sector, a new friction velocity $u_{*,r}$ can be obtained using Eq. (3). The standard wind can now be calculated using Eq. (4) with the new set of $z_0 = 0.05$ m and $u_{*,r}$.

The roughness length output from WRF (ZNT) was used for the generalization, but with some modifications for water grid points of the storm conditions. Over water, the roughness length z_0 has been calculated using the Charnock formulation

$$z_0 = \alpha_{ch} u_*^2 / g, \tag{5}$$

where α_{ch} has been chosen to be 0.018 in WRF. As discussed in [1] that the Charnock formulation might not be appropriate for the coastal waters, especially during storm conditions. An artificial enhancement of the roughness length is made by choosing a large value of the Charnock parameter α_{ch} to be 0.05, based on measurements from the offshore site Horns Rev.

In principle, winds at all levels can be used for the generalization because δr and δh are available at several heights. However, it should be noted that Eq. (5) has been derived for the surface layer close to the water surface where there is a direct connection between the wind and the water waves. It should also be remembered that Eq. (4) is also only valid for the atmospheric surface layer. To be specific, when we use winds at 10 m or 15 m, the friction velocity and the surface roughness are self consistent in the concept of surface layer. But when we use winds at 105 m, while there is no problem in applying Eq. (2), it can sometimes become questionable to use Eq. (4) because 105 m may well be above the surface layer, even though the boundary layer is quite deep during stormy conditions. The consequence is that u_* derived may deviate from the actual surface friction velocity, as will be shown to be true in Section 6.1. This leads to a biased G and consequently biased $u_{*,r}$ and eventually biased standard winds. Thus, in order to be faithful to the preconditions of the equations, surface winds have to be used to derive u_* even though we use winds at higher altitudes to correct the effects of orography and roughness changes.

For validation, the measured winds are also generalized through the microscale model LINCOM in WEng. The comparable surface conditions of the converted modeled and measured winds ensures a quantitative data validation.

The use of a linear model could imply high uncertainties in very complex terrain. The WAsP team from Risø suggests cautious use of

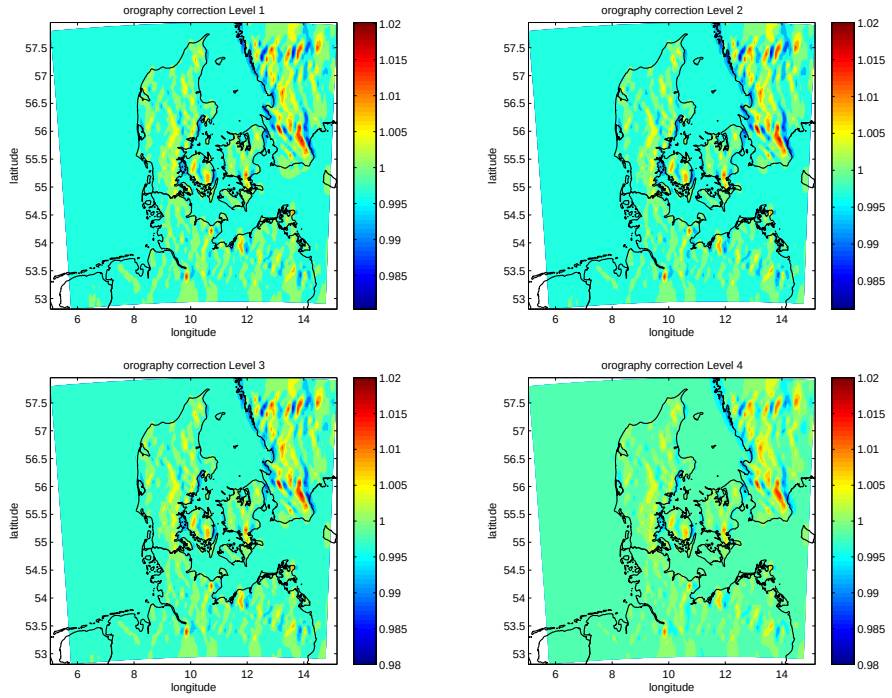

Figure 7: Correction factor for the orography δh, west sector, for elevation of 10 m, 15 m, 52 m and 105 m.

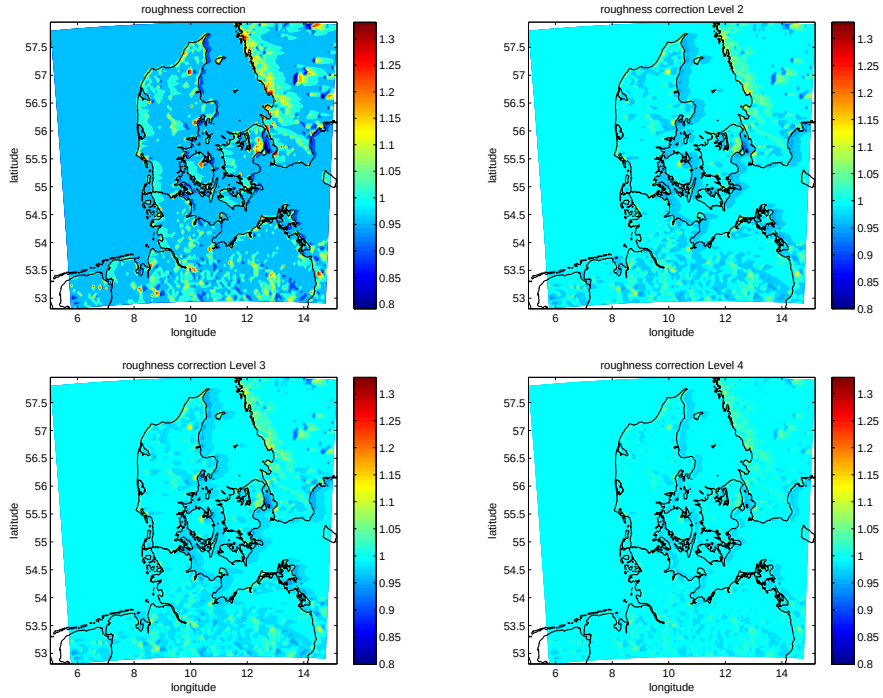

Figure 8: Correction factor for the roughness change δr, west sector, for elevation of 10 m, 15 m, 52 m and 105 m.

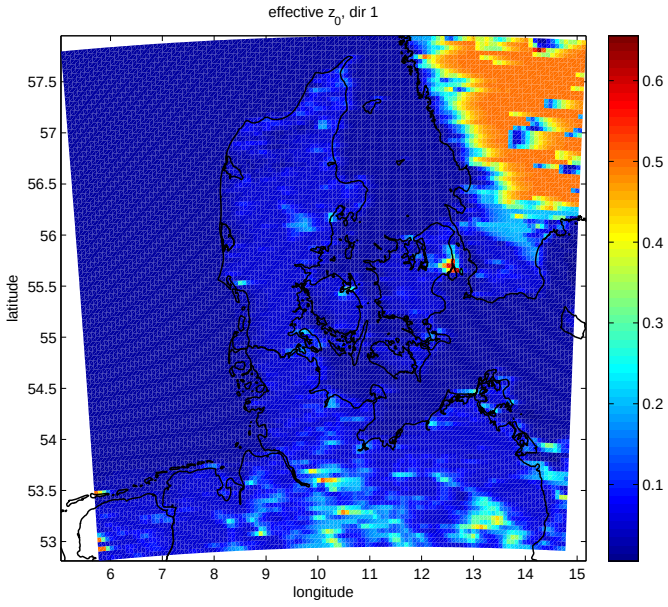

Figure 9: Effective roughness length z_0 (m) for the westerly winds.

the linear model for areas where RIX is beyond the range of -5% to 5%. The calculation of RIX is highly dependent on the upwind fetch used.

7 The statistical-dynamical downscaling method

The statistical-dynamical approach is based on carrying out a number of prescribed simulations to capture the mesoscale flow features caused by terrain. The simulations are not intended to reproduce any particular episode or weather event, indeed the simulations are quite artificial. The simulation yields information about the behaviour of the flow for different wind directions and speed. Compared to the method described in [10], where the extreme geostrophic winds from 12 sectors are extrapolated to the standard condition which later used as input to WEng, the statistical-dynamical method adds in mesoscale variability before the standard winds were calculated.

The approach used is an adaptation of the numerical wind atlas methodology, called KAMM/WAsP (described in [9]). The statistical-dynamical downscaling approach ([28]) has as its basis the assumption of a robust relationship between meteorological situations at the large-scale and meteorological situations at the small-scale. In the KAMM/WAsP methodology, so-called wind classes are defined that describe the large-scale wind climate.

Information about the large-scale meteorological situation has mainly in the past been taken from the NCEP/NCAR reanalysis data-set, [8]. This reanalysis dataset has been created by assimilating measurement data from around the globe in a consistent fashion from 1948 to the present day. The primary purpose for the generation of this data-set is to provide a reference for the state of the atmosphere and to identify any features of climate change. Another application of the dataset is as a long-term record of large-scale wind conditions. In the numerical wind atlas methodology the reanalysis data is used to create around 150 different large-scale wind situations, the wind classes, that represent the large-scale wind climate.

In order to make these wind classes meaningful at a smaller scale a mesoscale model is used to determine how the large-scale wind forcing is modified by regional scale topography. Therefore for each wind class a mesoscale model simulation is performed using the Karlsruhe Atmospheric Mesoscale Model (KAMM, [29]).

The modification that is made for the estimation of the extreme climate is to create extreme wind cases, instead of wind classes, to represent the extreme large-scale wind forcing from long term reanalysis data, instead of trying to represent a full climate. The statistical-dynamical downscaling methodology is intended to be even more efficient than the selective dynamical downscaling method.

For a particular area of interest extreme geostrophic wind cases are defined. A geostrophic wind time series is defined using the NCEP DOE AMIP II reanalysis data covering 30 years from 1980 to 2009 (see Section 4.1). From this time series the annual maximum geostrophic wind at low levels are determined for 12 direction sectors for each of 30 years. This results in 360 extreme geostrophic winds.

Each of the extreme geotrophic wind cases is used as a stationary forcing in the KAMM mesoscale model. Then for each mesoscale model

grid point the annual maximum method is used to calculate the 50-year wind. To cover a larger area a method is developed to account for variation in the extreme geostrophic wind cases with location.

7.1 Model description

The Karlsruhe Atmospheric Mesoscale Model (KAMM) is a 3D, non-hydrostatic, and incompressible mesoscale model. It is described in [29, 30]. Spatial derivatives are calculated in the model by central differences on a terrain following grid. The turbulent fluxes are modelled using a mixing-length model with stability dependent turbulent diffusion coefficients in stably stratified flow, and a non-local closure for the convective mixed layer. Lateral boundary conditions assume zero gradients normal to the inflow sides. On outflow boundaries, the horizontal equations of motion are replaced by a simple wave equation allowing signals to propagate out of the domain without reflection. Gravity waves can penetrate the upper boundary outward using the boundary condition of [31].

KAMM is able to run as a stand-alone model, i.e. the model can be run by using only the large-scale forcing in the form of a single vertical profile of geostrophic wind and virtual potential temperature. Hence, it is not necessary to nest the mesoscale model within a larger model that must supply the boundary conditions. At regional scales the mesoscale model is used to model atmospheric flows in domains of 100-1000 km x 100-1000 km in size with a typical horizontal resolution of 2.5 to 10 km.

In the vertical the model extends from sea level to 5500 m above sea level, using 25 model levels employing a terrain following coordinate system. The interval between vertical levels is not uniform. This allows for more closely spaced vertical model levels near to terrain. The first 5 model levels are at 0 m, 20.3 m, 58.7 m, 115.3 m and 190.0 m above the surface. The separation between these levels is smaller in elevated terrain.

The two areas of interest Denmark and Gulf of Suez are modelled within KAMM by defining domains that generously cover the area to be examined and locations where measurement data is available. Too great a proximity to the edge of the model domain has a detrimental effect on modelling results. The Denmark domain is 700 x 700 km and the Gulf of Suez domain is 500 x 800 km. The modelling is done in both cases with a resolution of 5 km.

Figures 10a and 11a shows terrain elevation for the modelling domains used for Denmark and Gulf of Suez extreme wind atlas studies respectively. The surface elevation data is derived from NASA's Shuttle Radar Topography Mission (STRM30) dataset version 2. The dataset can be accessed via the USA National Aeronautics and Space Administration (NASA) webpages. This data uses a longitude-latitude projection at 30 arc second resolution. This elevation data is manipulated first to change it to a UTM coordinate system and then to change to the resolution to that of the mesoscale simulations.

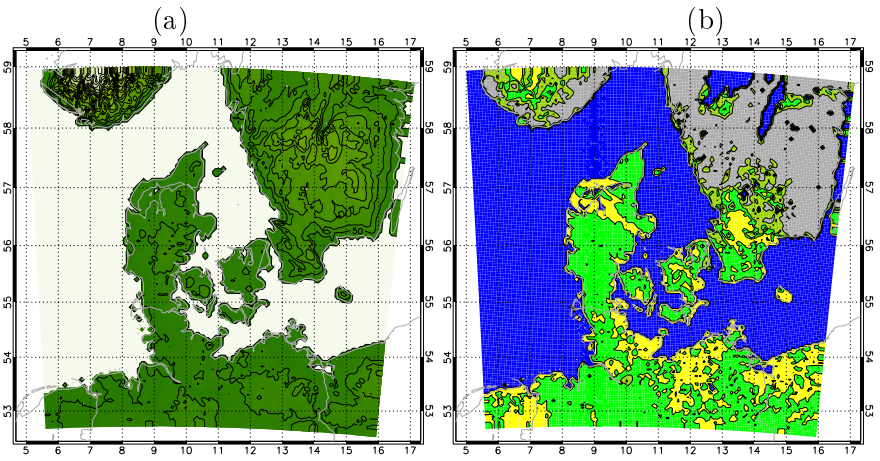

Figure 10: Maps showing (a) the surface elevation and (b) the surface roughness length over the Denmark modelling domain. Map axes are longitude and latitude. The contour interval is 50 m in (a) and in (b) the colour scale is: Blue $z_0 = 0.0002$ m, yellow $0.0002 < z_0 < 0.1$ m, bright green $0.1 < z_0 < 0.20$ m, green $0.20 < z_0 < 0.4$ m, grey $0.4 < z_0 < 0.60$ m. The model grid spacing is 5 km.

The map surface aerodynamic roughness length for the mesoscale modelling domains is shown in Figures 10b and 11b for Denmark and Gulf of Suez extreme wind atlas studies respectively. The aerodynamic surface roughness length data is derived from the United States Geological Survey (USGS) Global Land Cover Classification, also known as GLCC. The data can be accessed via a USGS webpages. By means of a look-up table, the land-use types were converted to aerodynamic surface roughness lengths. This roughness data is manipulated first to change it to a UTM coordinate system and then to change the resolution to that of the mesoscale simulations.

7.2 Extreme geostrophic wind cases

To repeat, a single KAMM mesoscale model simulation is forced with a single geostrophic wind profile (and virtual potential temperature profile). Within this methodology the geostrophic wind profiles are determined by identify, for each of 12 direction sector, the annual maximum geostrophic wind at 0 m from 1980 to 2009. The result of this process is 30 x 12 (360) extreme geostrophic wind cases.

The extreme geostrophic wind cases for the location 8.75 E 56.25 N are shown in Figure 12. This location is a mid point between the four reanalysis grid point at 7.5 E 55 N, 10 E 55 N, 7.5 E 57.5 N, 10 E 57.5 N. It is convenient to evaluate the geostrophic wind at the mid point, as it is based on the difference in pressure at the surround reanalysis grid points. Denmark is covered by approximately 5 of the reanalysis

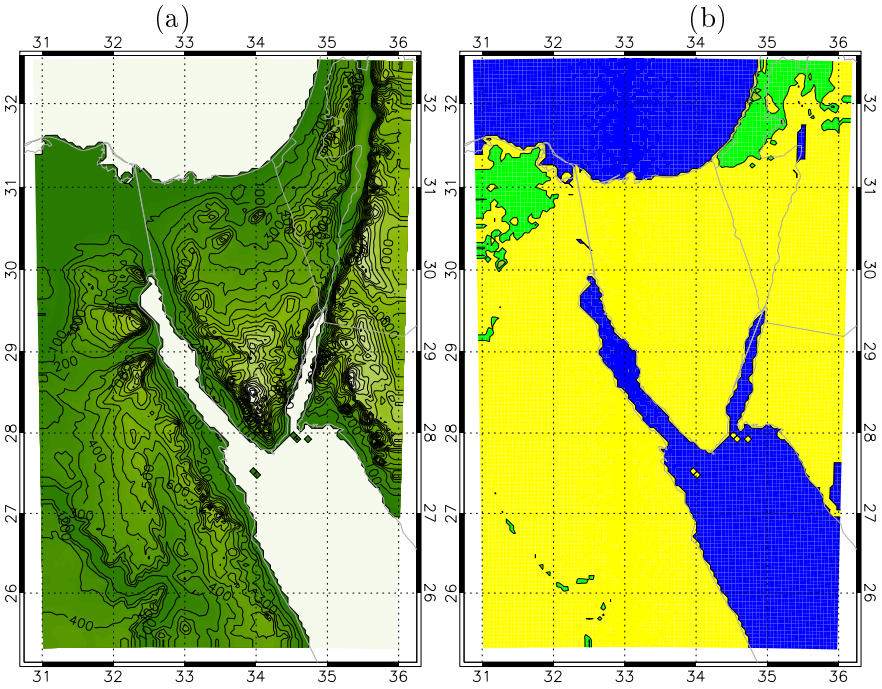

Figure 11: Maps showing (a) the surface elevation and (b) the surface roughness length over the Gulf of Suez modelling domain. Map axes are longitude and latitude. The contour interval is 100 m in (a) and in (b) the colour scale: Blue $z_0 = 0.0002$ m, yellow $0.0002 < z_0 < 0.1$ m, bright green $0.1 < z_0 < 0.20$ m, green $0.20 < z_0 < 0.4$ m, grey $0.4 < z_0 < 0.60$ m. The model grid spacing is 5 km.

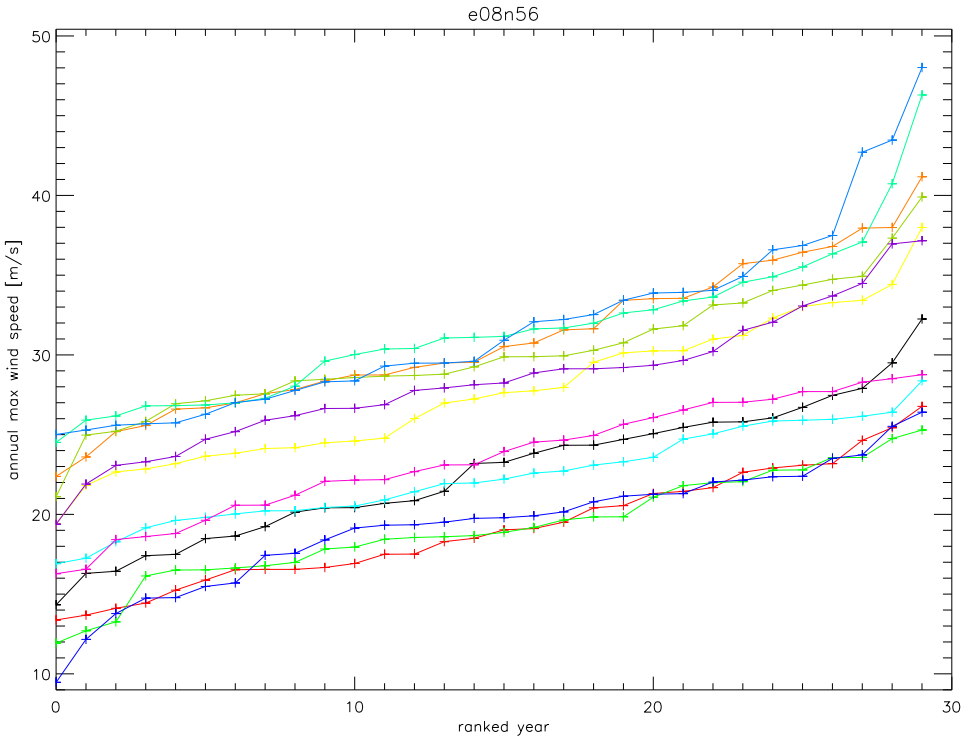

Figure 12: Plot showing 30 annual maximum geostrophic wind speeds for each of 12 direction sectors against ranked year at 8.75 E 56.25 N and used for the Danish study.

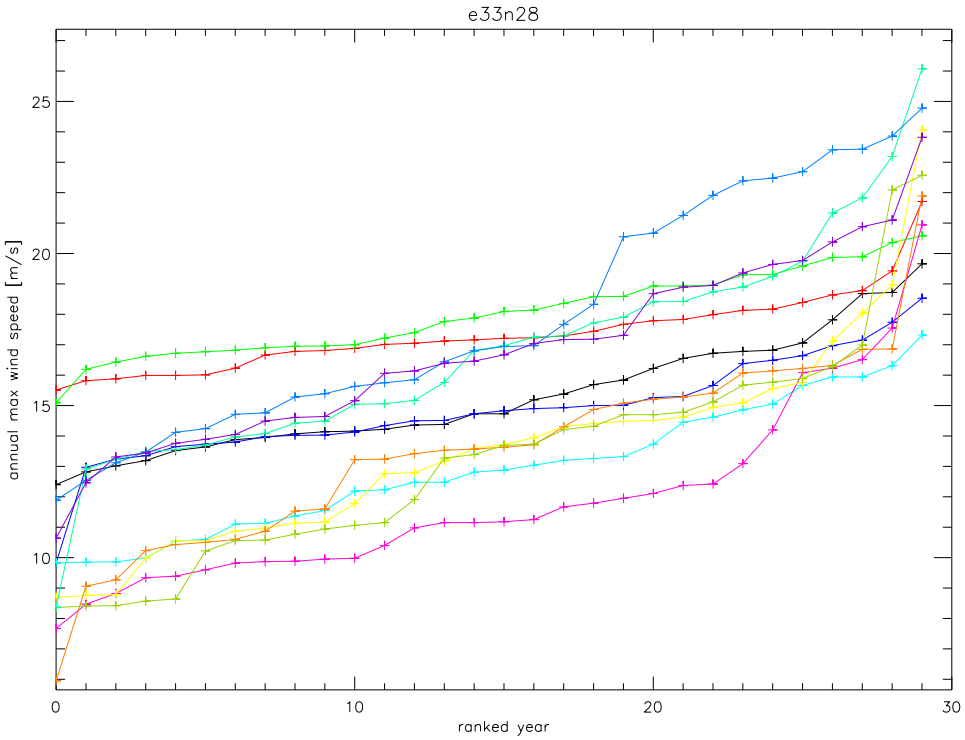

Figure 13: Plot showing 30 annual maximum geostrophic wind speeds for each of 12 direction sectors against ranked year at 33.75 E 28.75 N and used for the Gulf of Suez study.

Table 1: Denmark study NCEP DOE AMIP II mid-grid points annotation and 50-year sea level geostrophic extreme winds.

name	e06n53	e08n53	e11n53	e06n56	e08n56	e11n56	e06n58	e08n58	e11n58
longitude	6.25	6.25	6.25	8.75	8.75	8.75	11.25	11.25	11.25
latitude	53.75	56.25	58.25	53.75	56.25	58.25	53.75	56.25	58.25
50-y wind [m/s]	49.3	48.4	48.4	48.2	47.6	46.0	46.8	47.3	43.6

grid points, the Gulf of Suez is covered by 1 reanalysis grid point. In general, the variation of the actual extreme geostrophic wind cases should be determined and accounted for with the statistical-dynamical methodology.

For comparison, Figure 13 shows the extreme geostrophic wind cases for the location 33.75 E 28.75 N, which is the reanalysis mid-point best placed over Gulf of Suez, between 32.5 E 27.5 N, 35.0 E 27.5 N, 32.5 E 30 N, 35 E 30 N.

A summary of the extreme geostrophic wind cases is given in Figures 14 and 15 for Denmark and Gulf of Suez respectively.

Looking at Figure 14 is possible to (i). determine the variation of the extreme geostrophic winds over the areal extent of modelling domain used for Denmark and (ii). to determine the characteristics of how the extreme geostrophic winds vary with height for those cases.

There is a tendency for the extreme geostrophic winds to reduce slightly from west to east and the deep vertical characteristics of the extreme geostrophic winds are very different for westerly wind extremes and easterly wind extremes.

When moving from 0 to 5500 m, for westerly extreme geostrophic winds the geostrophic wind tends to increase with height, whereas for easterly wind extremes the geostrophic wind tends to decrease. This difference is associated with the structure of the tropospheric dynamic synoptic systems that produce the extreme wind events. The change of velocity with height is associated with a horizontal temperature gradient with a decreasing temperature northwards.

Figure 15 is a summary of the variation of the extreme geostrophic winds surrounding the Gulf of Suez. Moving from north to south (from 31.25 N to 26.75 N), the characteristic of westerly winds giving the highest extreme winds gives way to easterly winds having this role. At 33.75 E 28.75 N it is the northwesterly winds at the large scale that provide the highest extremes. The profile for the extreme geostrophic wind cases shows a general tendency for westerly winds to prevail. This effect appears to be stronger for locations eastward and southward.

7.3 Generalization of wind climate

The generalization of the mesoscale winds through the post-processing provides a basis for data validation. Measurement derived extreme wind climates are generalized in the same way to give the extreme wind for the same conditions (i.e. over a flat homogeneous surface with roughness length of 5 cm). Thus the local effects of a measurement

Figure 14: Figures showing the variation of the mean extreme geostrophic wind cases for different reanalysis points above Denmark. The location is given above each figure. Each colour represents data from a different direction sector, defined at 0 m. The distance from the centre of each figure represents the magnitude of the wind speed. Grey concentric circles mark 10, 20, 30, 40 and 50 m/s. The position of the lines also indicates the direction of the wind, e.g. westerlies appear at 9 o'clock and southerlies at 6 o'clock. The thick coloured lines show the change in the mean of the yearly extreme geostrophic vector wind at heights 0, 1500, 3000, 5500 m for each of the 12 wind direction sectors. If the coloured line is short, it means there is little change of the winds with height, i.e. a barotropic flow. If the coloured lines is long, it means there is a large change of winds with height, i.e. a baroclinic flow. The form of the line indicates the change in magnitude and/or direction of the winds with height. The data is from 9 NCEP DOE II reanalysis mid-grid points determined for the period 1980-2009 (30 years). The extreme is determined by the yearly maximum geostrophic wind at 0 m. The standard deviation of u and v component winds of the sectorwise yearly extreme geostrophic wind over the 30 year period is given at 0 m (bold line box) and at 5500 m (light line box). The black lines give the estimate of the 50-year extreme geostrophic wind at 0 m for each sector based on annual maximum method.

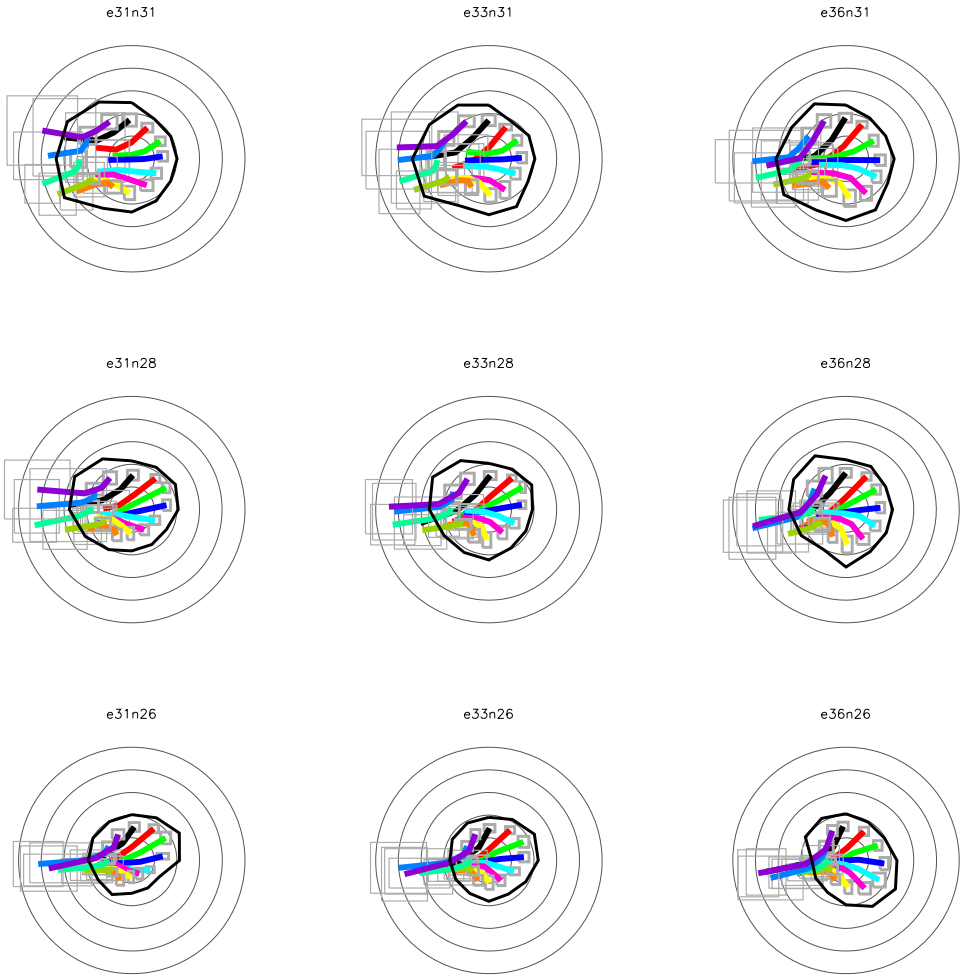

Figure 15: As in Figure 14 except for the 9 NCEP DOE II reanalysis mid-grid points, covering the Gulf of Suez modelling domain

Table 2: Gulf of Suez study NCEP DOE AMIP II mid-grid points annotation and 50-year sea level geostrophic extreme winds.

name	e31n26	e33n26	e36n26	e31n28	e33n28	e36n28	e31n31	e33n31	e36n31
longitude	31.25	31.25	31.25	33.75	33.75	33.75	36.25	36.25	36.25
latitude	26.25	28.75	31.25	26.25	28.75	31.25	26.25	28.75	31.25
50-y wind [m/s]	23.6	27.6	33.6	23.1	27.5	32.5	24.8	28.0	31.2

site's surface roughness length changes and orography can be removed (consider how extreme wind may be modified by orographic speed up at a hill top measurement site).

The generalization method also allows mesoscale model derived extreme wind statistics to be further downscaled through microscale modeling to determine local extreme wind climate at specific places. In this process microscale models are used to calculate the local effects at a site, which may significantly enhance or reduce the strength of the extreme winds.

The main aspects of generalization have been covered in section 6.3. The generalization is done on all generalized mesoscale surface winds from all of the extreme geostrophic wind cases' simulations. The input to the generalization is the 50 m a.s.l. wind speed and direction (as the generalization is direction sector depend) from each model grid point of mesoscale simulations, the output is the 10 m a.s.l. wind speed and direction for flat terrain with uniform roughness of 5 cm.

7.4 Disjunct correction

The reanalysis data is given with a 6-hour interval. Whereas the 50-year extreme wind should be based on consecutive 10-minute average winds, i.e. with a frequency of 6 recorded 10-minute winds per hour. Therefore there is a disjunct sampling error which needs to be address and corrected. The correction was based [12], based on an assumption of Guassian Markov chain, and has a sectorwise dependency based on climatologicall sector frequency of occurance.

In practice the correction was made by evaluating a sectorwise ratio of the $\frac{U_{max,T_d}}{U_{max,10-min}}$

$$\frac{U_{max,T_d}}{U_{max,10-min}} = b - a(\log_{10} x)^2 \tag{6}$$

where x is the frequence of occurrence and

$$a = 0.0209(T_d - \frac{1}{6})^{0.4627} \text{ and } b = 1 - 0.0342(T_d - \frac{1}{6})^{0.5436} \tag{7}$$

here $T_d = 6$ hours.

The correction is applied to the all generalized mesoscale surface winds by multipling it by ($1/\frac{U_{max,T_d}}{U_{max,10-min}}$) according to surface wind sector. This correction is done before any identification of annual maximum winds on the mesoscale grid, and thus before and Gumbel fitting is performed.

7.5 Adjustment method

From Figure 14 and 15 it can be seen that the extreme geostrophic winds vary across the region of interest. Therefore it may be advantageous to adapt the output from the simulations to reflect this variation. The method developed to achieve that is based on creating a sectorwise function of the mesoscale surface winds given the geostrophic wind

forcing for every mesoscale grid point. This can be thought of as an empirical geostrophic drag law approach based on mesoscale model output. That is

$$|u| = F(|G^{0m}_{isec}|) \tag{8}$$

where $|u|$ is the magnitude of mesoscale surface winds at 50 m a.s.l (above surface level) for a given G^{0m}_{isec} in sector $isec = 1, ..., 12$.

The first example of the function F was a simple linear regression

$$|u| = A|G^{0m}_{isec}| + C \tag{9}$$

where A and C are found by fitting data from the mesoscale simulations.

Another function was tried with the form

$$|u| = A_1|G^{0m}_{isec}| + A_2 P + C \tag{10}$$

where P is any another parameter further describing the extreme geostrophic wind forcing profile. From a limited set of candidates for P, it was found the best fitting was achieved with

$$P = |G^{1500m}_{isec}| - |G^{0m}_{isec}| \tag{11}$$

With A_1, A_2 and C determined for each direction sector for each mesoscale grid point (i.e. 12 x nx x ny functions in all, where nx and ny are the number of grid points in the x- and y-direction for the modelling domain) the dynamical mesoscale modelling is replaced with this function.

Now for any part of the domain the sectorwise extreme geostrophic wind for the nearest reanalysis grid point can be used to give the more locally relevant large scale forcing. Then the mesoscale surface winds at 50 m a.s.l are determined based on the function in Eq 10.

The results section will show results from the unadjusted and adjusted methodologies. To reiterate, the unadjusted methodology means that generalized mesoscale model wind speeds are used directly to assess extreme winds for any grid point in the mesoscale domain. The adjusted methodology means that an empirical drag law function relating the geostrophic wind to the surface winds is used to assess extreme winds for any grid point in the mesoscale domain. In the unadjusted methodology a single set of extreme geostrophic wind cases is used as forcing of the mesoscale model. In the adjusted methodology a single set of extreme geostrophic wind cases is used as forcing of the mesoscale model, for the purpose of fitting the empirical drag law function. Thereafter the empirical drag law function is employed with different sets of extreme geostrophic wind cases. The appropriate extreme geostrophic wind case is determined by the closest reanalysis mid-grid point in the mesoscale domain. For the measurement station locations the mid-grid points locations are given in Tables 3 and 4 respectively for Denmark and Gulf of Suez studies.

Table 3: Table linking the Denmark measurement station locations to the nearest reanalysis mid-grid point location.

Station	nearest mid-grid point location
Sprogoe	e11n56
Tystofte	e11n56
Kegnaes	e08n53
Jylex	e08n56
Risoe	e11n56
Hoevsoere	e08n56
Horns Rev	e08n56
FINO1	e06n53

Table 4: Table linking the Gulf of Suez measurement station locations to the nearest reanalysis mid-grid point location.

Station	nearest mid-grid point location
AbuDarag	e33n28
Zafarana	e33n28
El-Zayt	e33n28

8 The spectral correction method for mesoscale modeled winds

This method is aimed at correcting the general smoothing effect with mesoscale modeled winds in the application of extreme winds, which was mentioned in Section 2.4. The smoothing effect is demonstrated in Fig. 16 where the power spectra from the modeled winds miss the variability in the range from about 1 day^{-1} to higher frequencies, when compared with measurements. It was shown in [2] that the missed wind variability in the high frequency range is essential to the estimation of the extreme wind. A Gaussian process for the wind time series $u(t)$ has been used. It was derived that the annual maximum wind is a function of the zero- and second-order spectral moments m_0 and m_2:

$$\overline{u}_{max} = \sqrt{m_0}\sqrt{2\ln\left(\frac{1}{2\pi}\sqrt{\frac{m_2}{m_0}}T_0\right)} \tag{12}$$

The spectral moments are defined as:

$$m_j = 2\int_0^\infty \varphi^2(\omega)\omega^j S(\omega)d\omega, \tag{13}$$

where $S(\omega)$ is the power spectrum of the Gaussian process $u(t)$, $\omega = 2\pi f$; φ is a filter due to the temporal resolution given by $\varphi = \frac{\sin(\omega T_a/2)}{\omega T_a/2}$, with T_a the averaging time. With this filter, the integration of Eq. (13) is done from $\omega = 0$ to $\omega = 2\pi(1/(2T_a))$, i.e. the upper limit of the integration becomes the Nyquist frequency.

In order to correct the smoothing effect, we add the missed wind variability back to the spectrum of the modeled wind by replacing/filling the part with that matching the measurements.

If there are no measurements available, it was argued in [1] that the spectrum model with a slope of -5/3 can be used. This spectral model starts at a certain frequency f_c and ends at a frequency of required resolution up to the equivalent frequency of 10 min. Such a spectrum model with a -5/3 slope is based on numerous spectral analysis using measurements, numerical modeling and theoretical arguments, e.g. [32, 33, 34]. Based on long term measurements from mid-latitude flat terrains, it was found in [34] the following expression can well describe the power spectrum of wind speed:

$$S(f) = a_1 \cdot f^{-5/3} + a_2 \cdot f^{-3} \tag{14}$$

where $a_1 = 3{\cdot}10^{-4}$ m^{2}s$^{-8/3}$ and $a_2 = 3{\cdot}10^{-11}$ m^{2}s^{-4}. Even though the coefficients a and b change slightly with season where winter months corresponds to a greater a_2.

In the following we explain how the method is used in the absence (Section 8.1) and presence (Section 8.2) of measurements.

8.1 In the absence of measurements

It was also argued in [1] that in the absence of measurements, f_c can be chosen as 1 day^{-1}, according to the comparison of the measured and observed spectra. To make better connection to the physics of the weather, f_c was also recommended to be $1/T$, where T is the integral time scale of the wind time series, which represents the local weather scale. The spectral model, expression (14), is used.

8.2 In the presence of measurements

Instead of using expression (14), the power spectrum for the mesoscale range is used from the observed time series. Measurements for this purpose do not have to be long and are only needed to be long enough to cover the scale where the missing variability is. In [2], for the mid-latitude site of flat terrain, measurements of a couple of months are enough for this purpose because the interannaual and seasonal variability of the mesoscale power spectrum is not significant [34]. It should be noted that this method has also been applied to coarser resolution model data, i.e. the NRA-2 extreme winds. For this application, it happens that the NRA-2 data misses the variability to greater scales, compared to the mesoscale modeled data. This will be shown in Section 10 where we correct the extreme winds derived from the method described in Section 2.3 using NRA-2 data. Compared to flat terrains, the spectral behavior in complex terrains is found to contain more energy in the frequency range $10^{-5} < f < 10^{-3}$ Hz [35].

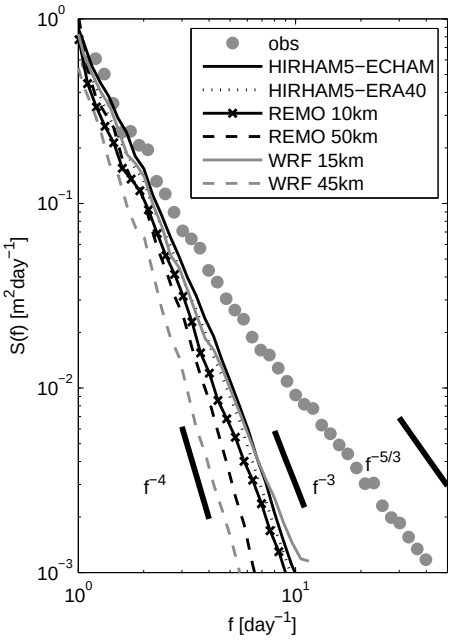

Figure 16: Spectra of 10 m wind speed at Horns Rev from measurements and six model simulations Thick short straight lines show the three reference slopes -5/3, -3 and -4. This plot is from [2].

9 Results, validation and discussion: the extreme wind atlases in flat and medium complex terrains

9.1 From the selective dynamical downscaling method

The extreme wind atlases for the three areas are made, including the 50-year wind obtained from several model levels without post-processing and the 50-year wind at standard conditions.

In the discussion we will cover the following topics: (1) The variations introduced by using wind output from several levels, with particular concern in the application of the post-processing procedure. (2) The change introduced by using data from particular years. In particular, we discuss the updated results by including the storms from 2011, in comparison with the published results as in [1].

The statistical uncertainties related to the climatological representativity of the modeled period and the length of the data will be discussed particularly in Section 11.

9.1.1 The flat terrain - Denmark

The extreme wind atlases at 15 m calculated with yearly strongest storms 1999 - 2011, with and without post-processing, are presented in Figure 17. The results at 8 sites (7 from Denmark, 1 from Germany) are compared between the measured and modeled 50-year wind (Table 5).

In comparison with the results obtained using storms modeled in the period of 1999 - 2010 (period I), there is some difference in the results obtained by including the new storms from 2011 (period II, 1999 - 2011). The differences in the 50-year wind between the two periods are plotted in Figure 18 for with- and without- the post-processing; here the wind outputs at 15 m have been used. It can be seen that the pattern of changes caused by including storms from 2011 are consistent for U_{50} and $U_{50,st}$. Over most part of the domain the changes are quite small (green to yellow colours) but there are also quite a big area the 50-year wind is considerably greater by including the storms from 2011 (the blue areas).

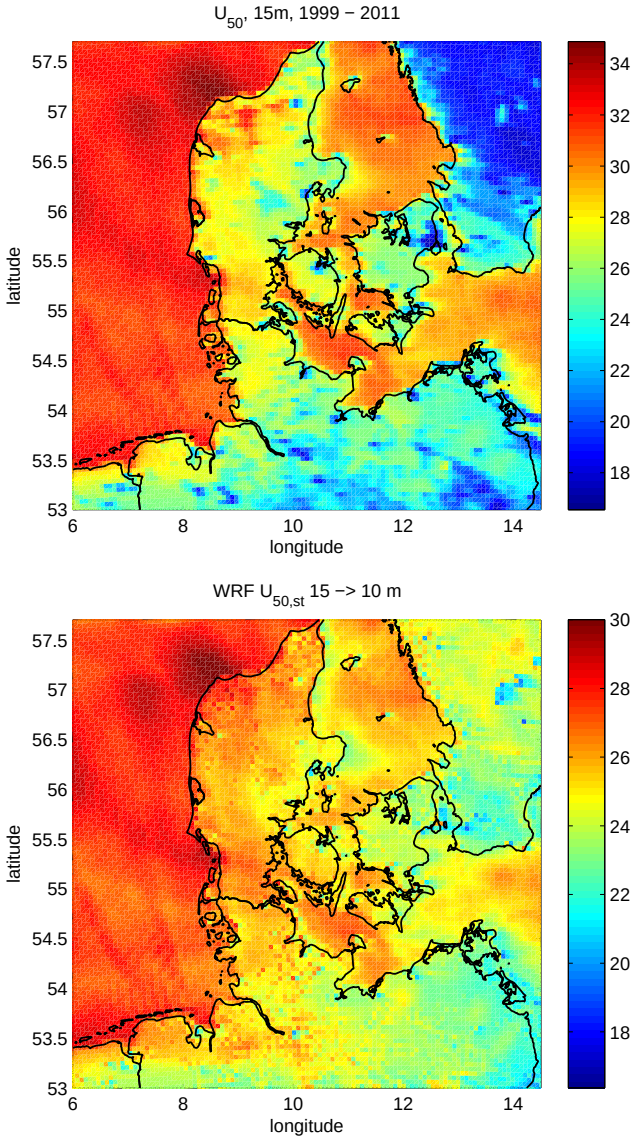

Figure 17: Maps of the 50-year wind over Denmark and surroundings, storms from 1999 - 2011 are used. (a), above, U_{50}, the 50-year wind at 15 m calculated with 15 m wind speeds from the WRF model output. (b), below, $U_{50,st}$, the 50-year wind of the standard conditions through the post-processing procedure: at 10 m and over homogeneous surface with roughness length 5 cm.

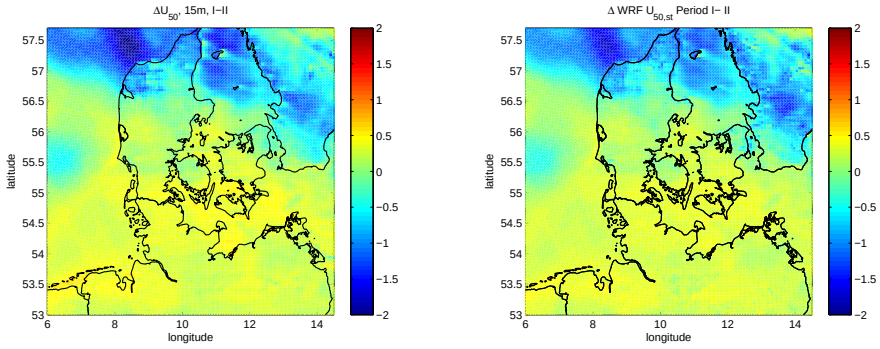

Figure 18: The difference in the 50-year wind (U_{50}, left) and 50-year standard wind ($U_{50,st}$, right), calculated using storms 1999 - 2010 and 1999 - 2011. Winds at 15 m were used.

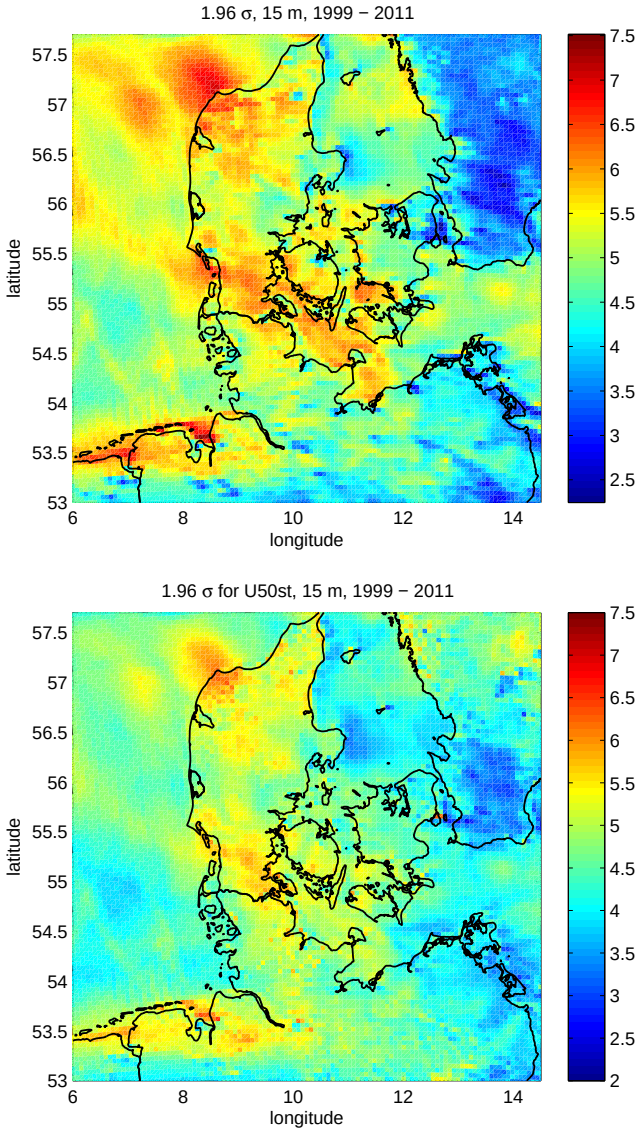

Figure 19: The distribution of the 95% confidence interval for U_{50} and $U_{50,st}$: $1.96 \cdot \sigma(U_T)$ from simulated storms 1999 - 2011. Winds at 15 m were used.

Table 5: The 50-year wind ms^{-1} at measuring height, $U_{50} \pm 1.96\sigma$, and the 50-year standard wind, i.e. at 10 m, over roughness of 0.05 m, $U_{50,st} \pm 1.96\sigma$, observed and simulated, and their difference $\Delta U_{50} = U_{50}$(WRF)-U_{50}(OBS), for Denmark (A) and Gulf of Suez (B) cases. *: values from [10]. x: Corresponding values one and two grid points away from the coast are 20.8 and 21.2 ms^{-1}. +: The corresponding values one and two grid points away from the coast are 16.3 and 17.1 ms^{-1}.

		U_{50}, no generalization				$U_{50,st}$, with generalization		
	Stations	Height (m)	WRF	OBS	ΔU_{50}	WRF	OBS	$\Delta U_{50,st}$
A	Sprogø	70	34.2 ± 6.7	33.0 ± 3.7	1.2	24.2±4.4	23.9±2.0 *	0.3
	Tystofte	39	31.2 ± 6.6	31.5 ± 4.5	-0.3	25.0±5.4	25.7±2.9 *	-0.7
	Kegnæs	23.4	31.2 ± 7.0	35.8 ± 7.0	-4.6	25.8±5.5	26.3±3.8 *	-0.5
	Jylex	24	31.8 ± 6.4	35.4 ± 5.5	-3.6	27.4±5.4	29.1±2.9 *	-1.7
	Risø	76.6	32.0 ± 6.3	33.2 ± 5.4	-1.2	25.6±5.3	23.7 ± 4.7	1.9
	Høvsøre	100	39.5 ± 8.0	44.6 ± 12.5	-5.1	29.7±5.8	29.8 ± 9.4	-0.1
	Horns Rev	62	39.3 ± 7.7	44.2 ± 14.0	-4.9	29.0±5.3	31.6±8.5	-2.6
	FINO1	50	36.5 ± 6.0	38.1 ± 8.8	-1.6	27.8±4.3	27.4±7.6	0.4
B	Abu Darag	24.5	25.7 ± 5.8	26.6 ± 4.0	-0.9	20.5±4.8	20.2±3.4	0.3
	Zafarana	24.5	25.4 ± 5.3	28.1 ± 4.4	-2.7	19.9±4.1	19.8 ± 2.8	0.1
	El Zayt	24.5	20.0 ± 2.2 (x)	24.5 ± 3.4	-4.5	15.5±1.9(+)	17.4±2.6	-1.9

This impact of storms from individual year was examined by plotting the annual wind maxima over the whole area year-by-year in Figure 20 and 21. It is clear that the year-to-year variability of the yearly maximum winds is significant and the last subplot of Figure 21 clearly explains the differences shown in Figure 18. As will be discussed more in Section 11 that the estimation of the 50-year wind will be affected by the data length but also by the period which describes the extreme wind climatology used for the estimation. In [1], their figure 9c shows that the natural variation in U_{50} by using different period can be as high as 2 ms^{-1}, based on the 28 year measurements at 39 m, at Tystofte. This magnitude of 2 ms^{-1} is, however, quite small compared to the fitting uncertainties which is 4.5 ms^{-1} when using 28 years of data (their table III). This fitting uncertainty related to the Gumbel distribution is defined as the 95% confidence interval here and it is calculated as $1.96\sigma(U_T)$ where U_T is U_{50} here and $\sigma(U_T)$ is

$$\sigma(U_T) = \frac{\pi}{\alpha}\sqrt{\frac{1 + 1.14k_T + 1.10k_T^2}{6n}} \tag{15}$$

with

$$k_T = -\frac{\sqrt{6}}{\pi}\left[\ln\ln\left(\frac{T}{T-1}\right) + \gamma_E\right], \tag{16}$$

according to Mann et al. [36].

Obviously, $\sigma(U_T)$ is greater at smaller n and α. According to the estimation of α:

$$\alpha = \frac{\ln 2}{2b_1 - \overline{U^{max}}} \tag{17}$$

where $\gamma_E \approx 0.577216$ is the Euler constant, $\overline{U^{max}}$ is the mean of U_i^{max} and b_1 is calculated from

$$b_1 = \frac{1}{n}\sum_{i=1}^{n}\frac{i-1}{n-1}U_i^{max}, \tag{18}$$

the value of α depends heavily on the relative relation between the weighted annual wind maxima from each year sorted in ascending order and the mean of the annual wind maxima through the years.

The fitting uncertainties for U_{50} and $U_{50,st}$ calculated from 1999 - 2011 are plotted in Figure 19. Even though for each grid point, the data length n is the same (13 years), the fitting uncertainties range from only a couple of meter per second to more than 7 ms^{-1} in some areas. We could see that the strong storms from 2011 have partly contributed to the large fitting uncertainties north-west of Denmark; we could also find similar patterns in Figure 19 that very likely are related to the strongest storms from some other years, e.g. 1999 and 2006, certainly caused by the relative relation of $2b_1$ to $\overline{U^{max}}$. This strongly demonstrates that the longer period of data, the more reliable the estimation.

There is also a systematic difference in $U_{50,st}$ when using winds at different heights. Figure 22 shows that the spatial distributions of $U_{50,st}$ are similar when winds at 10 m or 15 m were used. However,

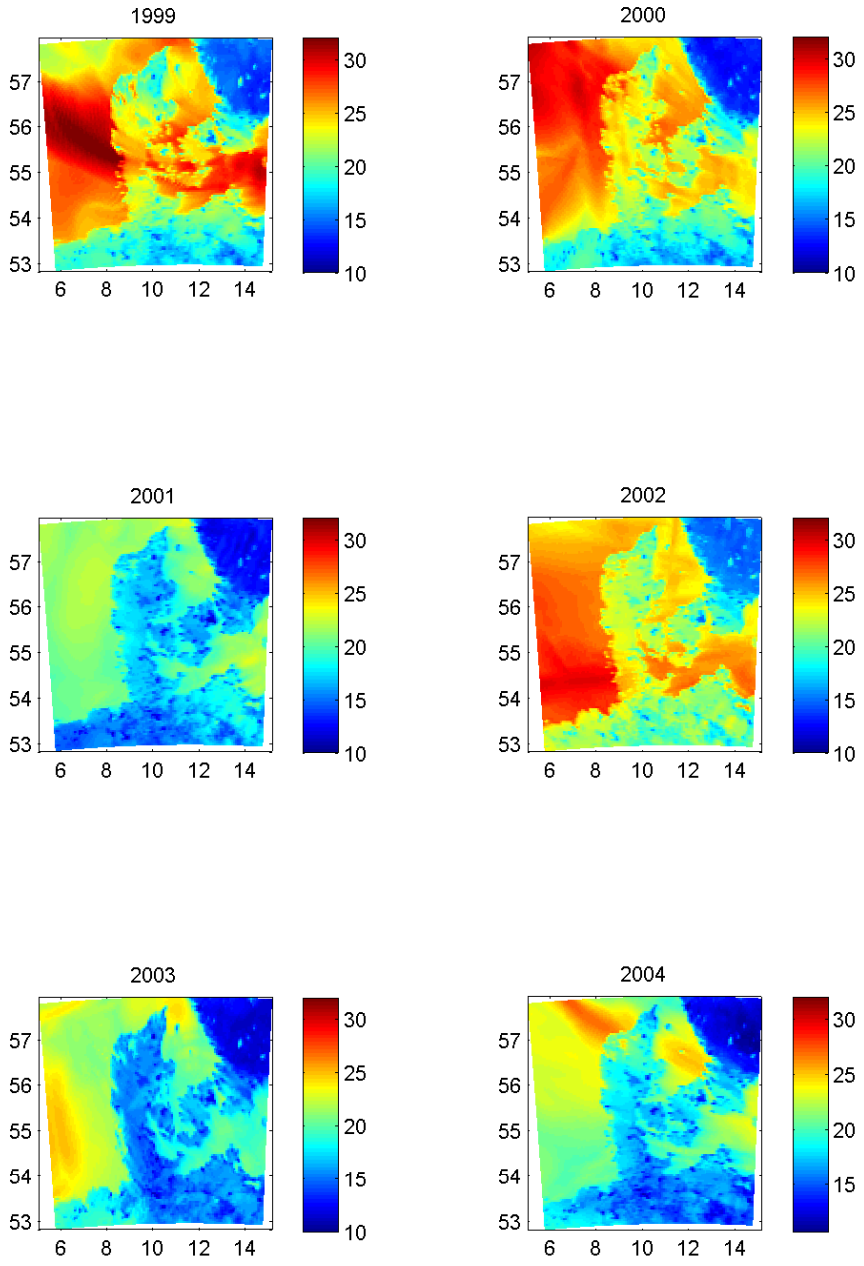

Figure 20: The distribution of the yearly U_{max} from simulated storms over Denmark.

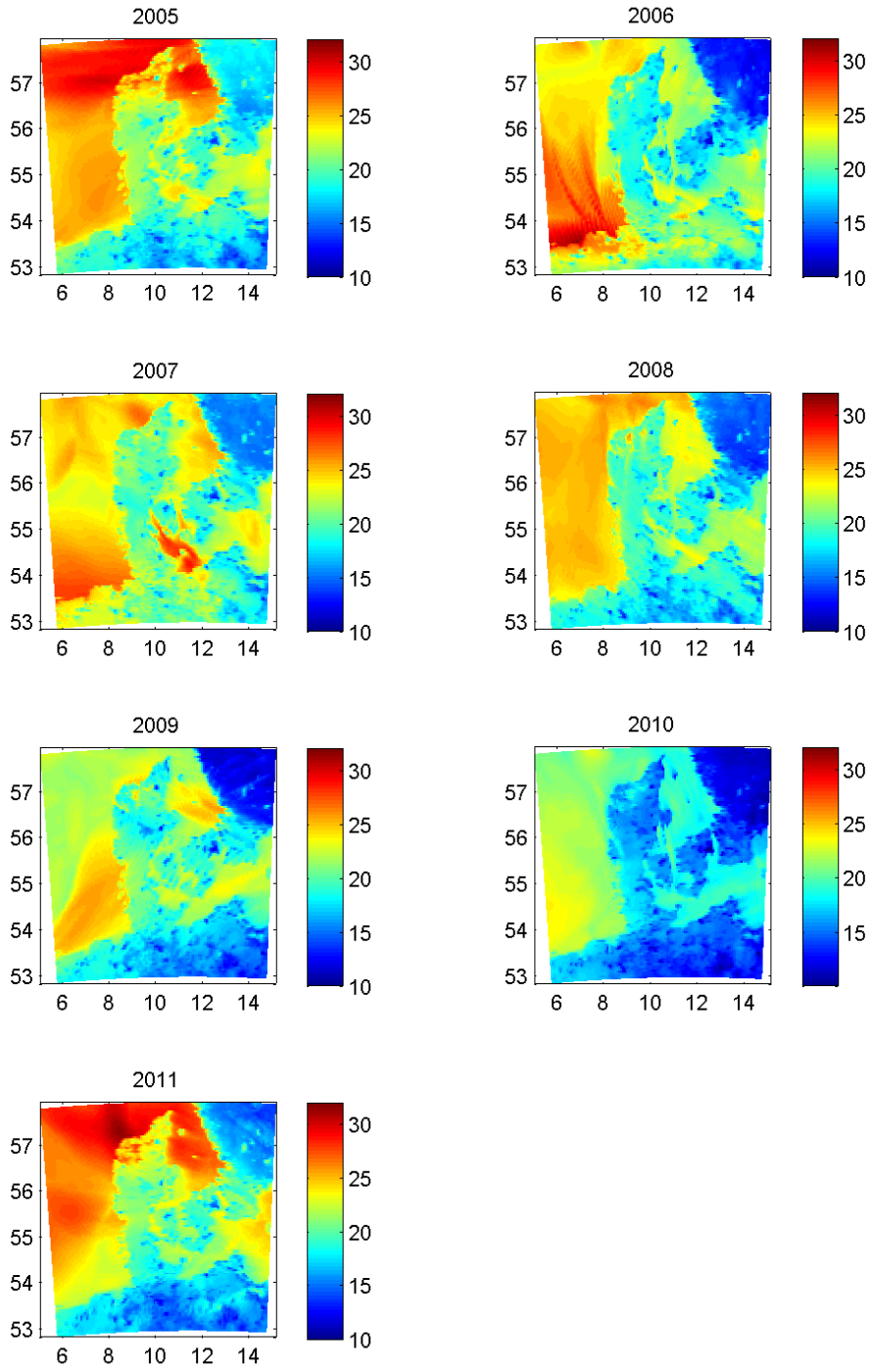

Figure 21: The distribution of the yearly U_{max} from simulated storms over Denmark.

using winds at 15 m gives a systematically smaller values of about 0.2 ms^{-1} over land and about 0.5 ms^{-1} over water. Compared to the results obtained from 15-m wind, $U_{50,st}$ are even smaller over water when winds at 105 were used, although the differences over most land grids are still rather small and for areas of high roughness length, the correction seems to be overdone using 105-m winds, leading to considerably larger values of $U_{50,st}$.

In order to understand this systematic bias, there are two facts that need to be reviewed. One fact has been mentioned in Section 6.3 that when calculating u_* using Eq. (4), the wind speed used has been assumed to be in the surface layer where this scaling law is valid. The higher level we use, the higher chance that the winds are above the surface layer. The systematic decreasing in u_*, as shown in Figure 23, supports this argument. From this plot, it can be seen that the contrast of u_* between land and the North Sea at 52 m and 105 m has been smoothed out, in comparison with 10 and 15 m. This is in consistency with the corresponding wind field where it is less affected by the surface at higher altitudes. Remembering u_* is a surface scaling parameter that should be closely related to the surface roughness, we may argue the winds at 52 and 105 m are not appropriate for the generalization procedure developed here, unless the generalization procedure will be modified that G can be linked to winds above the surface layer, and the ultimate use of $U_{50,st}$, as designed for WEng, will also be revised. Another feature clear in Figure 23 is that the changes in u_* is not large over land. We believe that this reflects the general difference in the boundary layer structures over land and water. Over water, due to the much smaller roughness length, the boundary layer and hence the surface layer is much shallower and winds at the similar levels (here, 15 m, 52 m and 105 m) have larger chance to be above the surface layer in comparison with the land conditions.

Another source for the difference using 10-m and 15-m winds is that 10 m here is not a model level but a diagnostic level. That means the winds at 10 m were calculated from winds at the first model level, namely 15 m, using the surface layer scheme embedded in WRF, here the Monin-Obukhov scheme.

The difference in $U_{50,st}$ by using winds at 10 m and 15 m is quite small compared to the fitting uncertainties as shown in Figure 19. We conclude that both 10 m and 15 m winds are suitable.

All our measurements are from zones where the changes, either due to using different periods or due to using winds at 10 m or 15 m, are not significant (Figure 18).

9.1.2 The channeling terrain - Gulf of Suez

This area is chosen because of its special meteorological mesoscale channeling effect that contributes to the extreme wind climate. This is quite different from the Denmark case where the synoptical low system is the cause to the extreme winds. The meteorological mechanism here is the mesoscale channeling, at the first glance. This brings the chal-

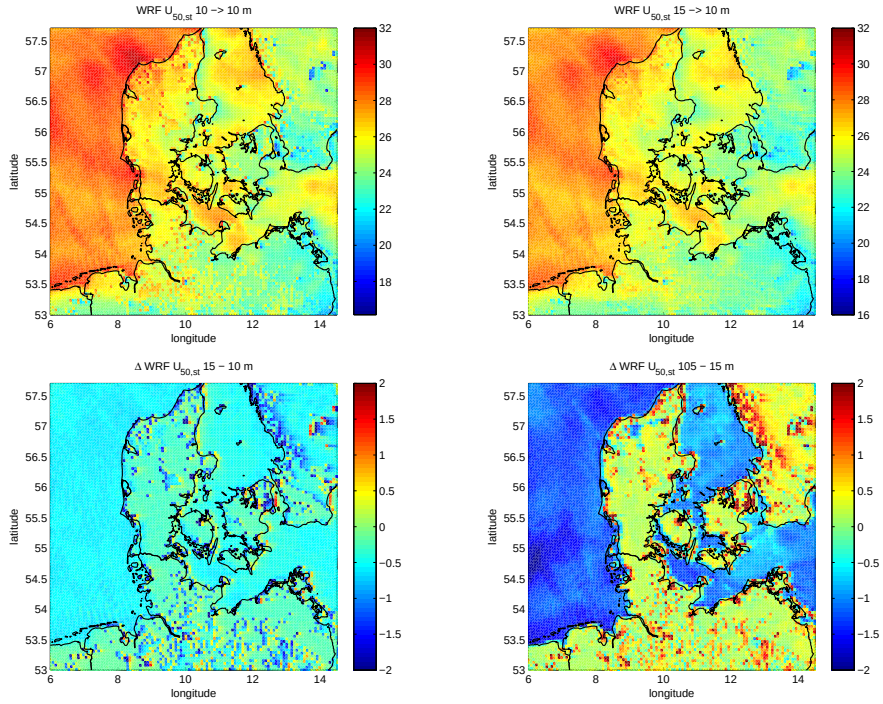

Figure 22: Map of the 50-year standard wind over Denmark and surroundings, obtained from storms modeled during 1999 - 2011. The modeled winds at 10 m were used in the plot to the upper-left and the winds at 15 m were used in the plot to the upper-right. The below-left plot shows the systematic difference of $U_{50,st}$ caused by using the data at 15 m and 10 m and below-right shows the difference of $U_{50,st}$ using WRF output winds at 105 m and 15 m.

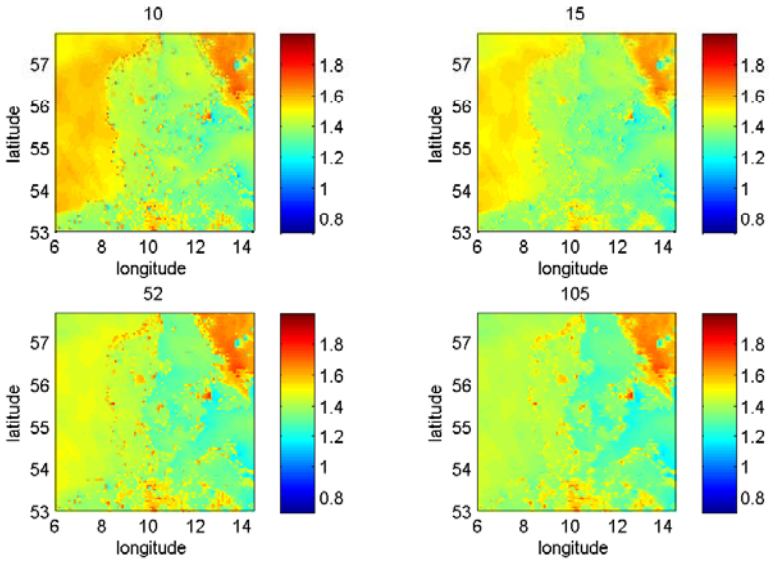

Figure 23: u_* that are used in Eq. (4) to obtain the wind of standard conditions, obtained using the WRF output winds at 10 m, 15 m, 52 m and 105 m, respectively.

lenge to the methodology at the first step where there is a high chance that the NRA-2 data do not contain the channeling winds so that the events are not identified. Luckily that the channeling effect is closely related to the synoptical pressure gradient over a large area containing the model domain III. For the overlapping period of measurements and simulation, 80% of the annual strongest storms are identified. The 20% mismatching cases are partly due to short duration of some events (shorter than 6 hours, which is the temporal resolution of the NRA-2 data) and partly due to missing measurements. As shown in [1], the data coverage of measurements at the Gulf sites ranges between 78% and 86%. When there are big holes in the measurements, the NRA-2 data can compensate.

The terrain in this area, as introduced in section 4.3 (also figure 3b and d in [1]), is quite complex but not as complex as in the Navara region (next section), especially for the locations of the measurement sites along the channel. However, all measurements are located along the coastline, which is a different kind of complexity from that in the mountainous areas as in Navara.

The maps of the 50-year winds, with and without the post-processing, are presented in Figure 24. For particular sites, the results are listed in [1] ((Table 5)). It was discussed in details there how the resolution could be sensitive along the coastline. For the sites where relatively long term measurements ($>$ 7 years) are available, the overall agreement of the 50-year wind is good and the improvement in data val-

idation is quite clear through post-processing. Moving the reference point for the simulated data one or two grid points (3 or 6 km) away or closer to the coastline can sometimes affect the validation results if the site is very close to the coastline.

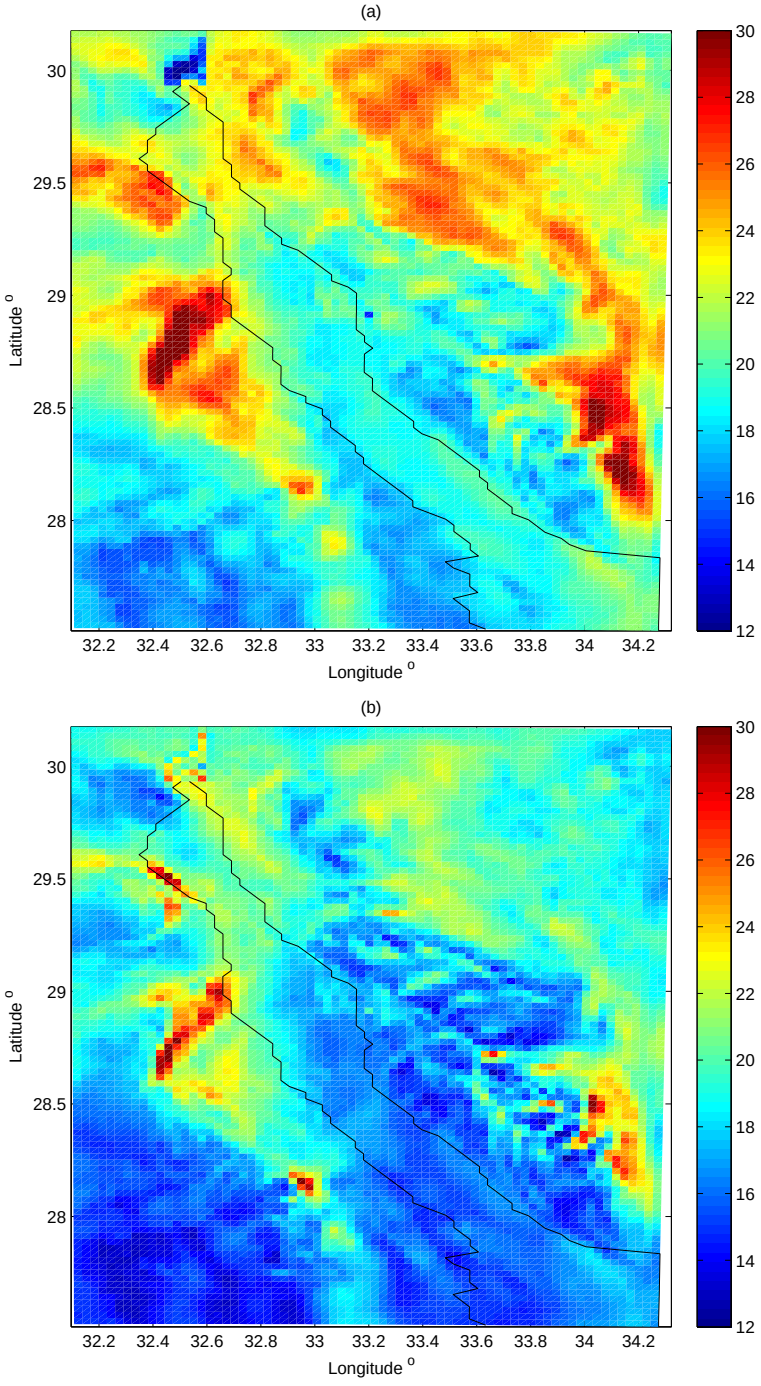

Figure 24: Same as Figure 17 but for the Gulf of Suez.

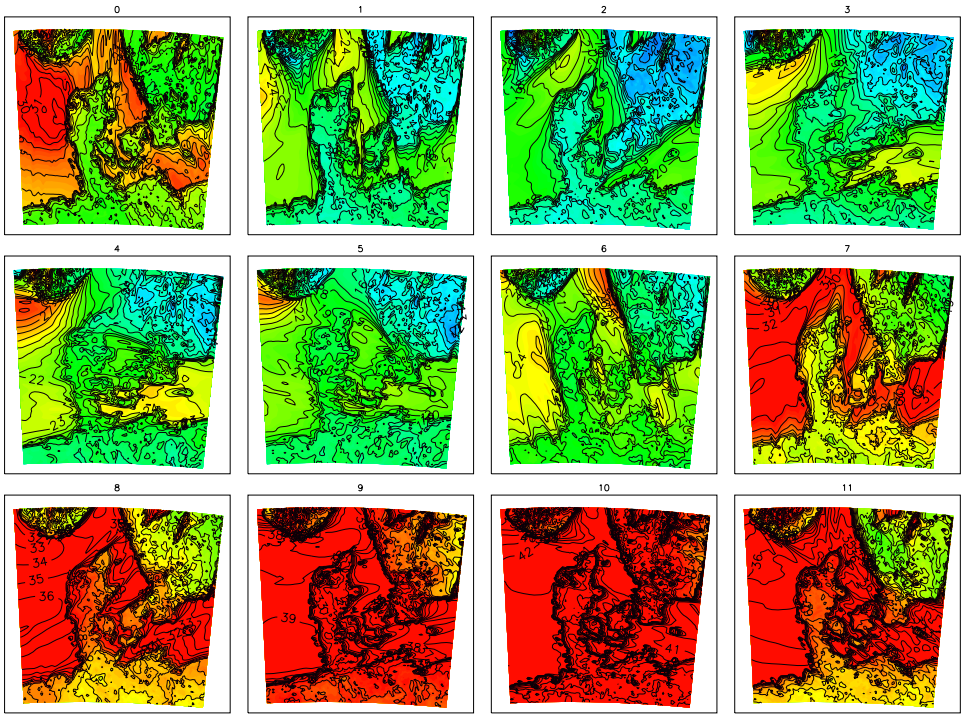

Figure 25: Sectorwise 50-year extreme winds at 50 m a.s.l. for Denmark.

9.2 From the statistical-dynamical downscaling method

A single extreme wind climate estimation is created by application of the 360 extreme geostrophic wind cases as forcing to the KAMM mesoscale model. Mesoscale surface winds are calculated for 30 simulations for each of the 12 direction sectors. For the Denmark study, the extreme geostrophic wind cases at e08n56 was used initially, but as part of the investigation of the method, extreme geostrophic wind cases at e06n53, e08n53 and e11n56 were also used.

The maps shown in Figure 25 shows the estimate of the 50-year extreme wind at 50 m for each directions sector for Denmark. The estimate is based on the the annual maximum method, using the result from each of the forcing sectors separately.

The maps shown in Figure 26 shows the estimate of the 50-year extreme wind at 50 m for each directions sector for Gulf of Suez.

There are two aspects of these maps that need to be considered. The first is that the actual simulated wind direction at each of the mesoscale grid points is not necessarily in the same direction sector as the geostrophic forcing wind. This is especially likely to be the case for the Gulf of Suez study, where channelling effects play an important role, and lead to a drastic difference in wind forcing direction and surface wind direction. Second the wind speed in the maps cannot be directly compared to measurement because local effects of orographic

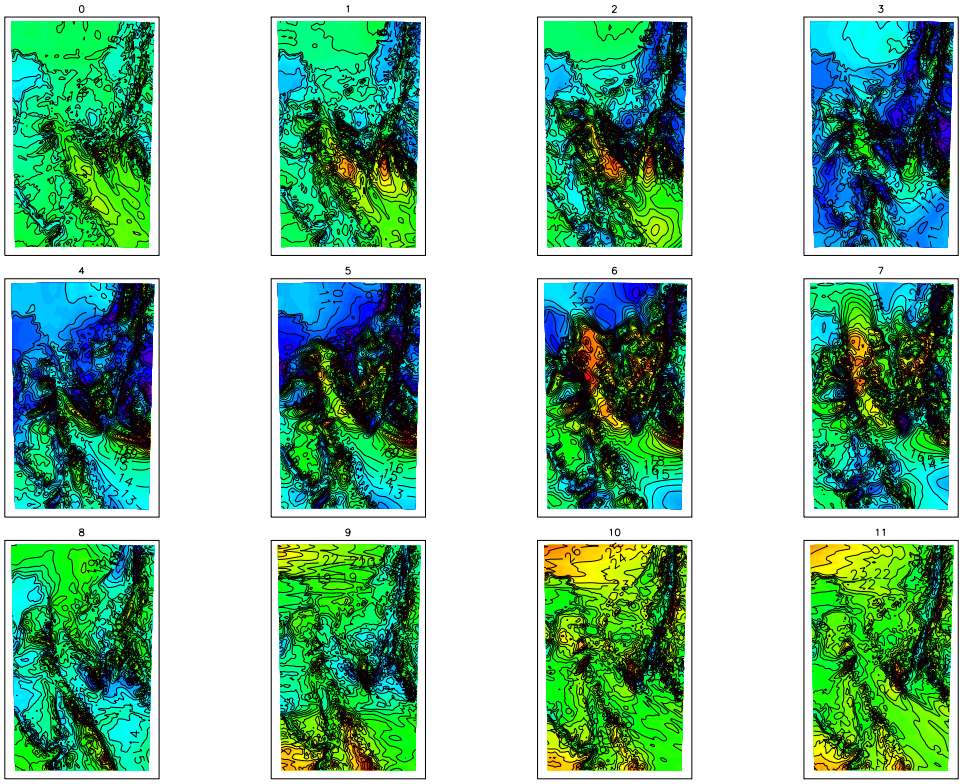

Figure 26: Sectorwise 50-year extreme winds at 50 m a.s.l. for Gulf of Suez.

speed-up and roughness changes are not included, because of unresolved terrain description absent in the mesoscale modelling. It is for this reason the wind generalization process is carried out, and therefore the generalized extreme wind climate is presented in subsequence maps.

Figure 27 shows the 50-year extreme wind at 10 m a.s.l. for the Danish study based mesoscale modelling of the cases from e08n56, using the unadjusted method and the adjusted method. One of the interesting features that appears in the adjusted method map but not in the unadjusted method map, is the local maximum around the German Bight. This increase in the extreme wind map be due to a mesoscale effect in combination with a different set of extreme geostrophic wind cases, used in the the linear function (Eq 10).

Therefore another set of mesoscale simulations was carried out using the extreme geostrophic wind cases derived at e06n53, which lies above the German Bight. The result of this extreme wind climate calculation are shown in Figure 28. Interestingly the German Bight feature is again present in these results, suggesting that it is a robust feature, although somewhat displaced to the northwest in this case. Also the feature is present in the unadjusted method and adjusted method. This is to be expected, as only small difference in the two methods should be seen in the region of the location where the extreme geostrophic wind cases are defined. Any differences there are due to the limitation of and uncertainty introduced by the linear empiral drag law function Eq 10 .

Later the validation will show that there tended to be an underestimate of the extreme wind climate for the offshore sites. Therefore simulations were performed with increased surface roughness for water within the generalization step. Best results were found for cases defined at e06n53 and e08n53 and water roughness $z0w = 0.02$ m. These are shown for completeness in Figures 29 and 30.

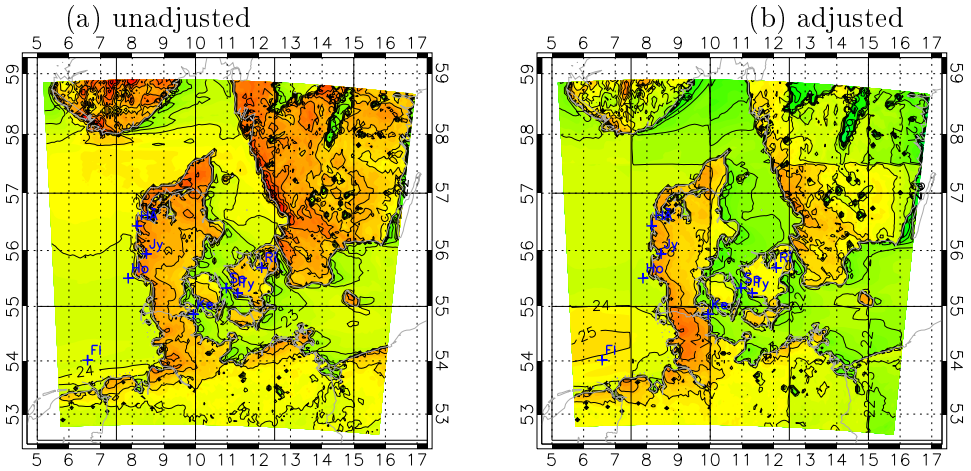

Figure 27: Maps showing the estimated 50-year extreme wind for Denmark and surroundings at 10 m a.s.l. from (a) the unadjusted methodology and (b) from the adjusted. The extreme wind cases were based on location e08n56 and the water roughness, $z0w = 0.0002$ m. The solid grid lines indicate the partions between the reanalysis grid points. The blue annotations indicate the measurement station locations, accompanied by the first two letters of the station name.

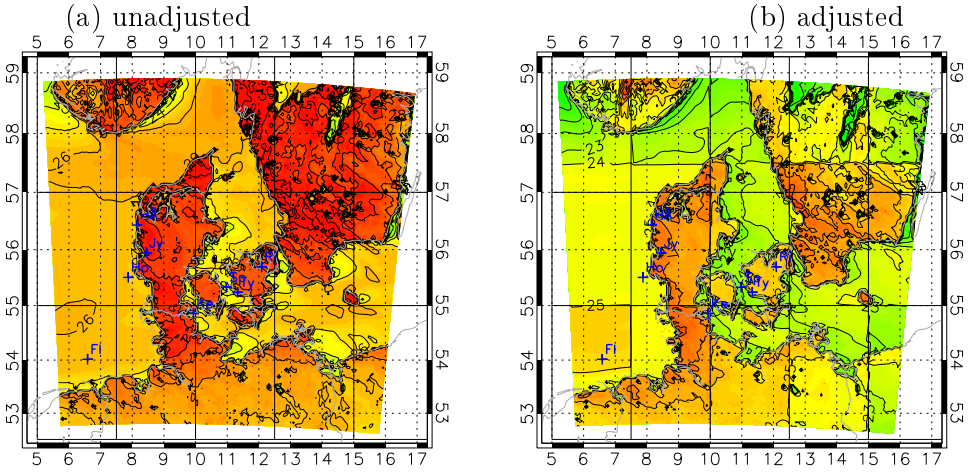

Figure 28: As in Figure 27 except for extreme geostrophic wind cases based on e06n53.

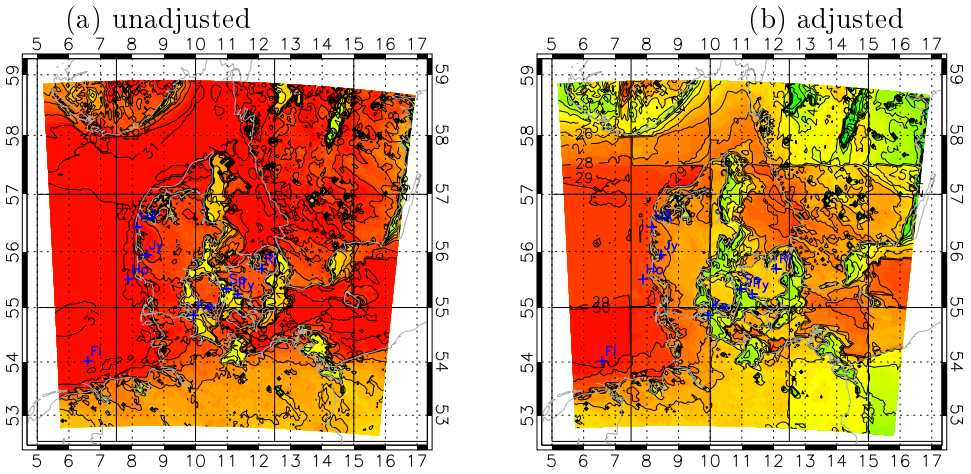

Figure 29: As in Figure 28 except for an increase water roughness, $z0w$ = 0.02 m.

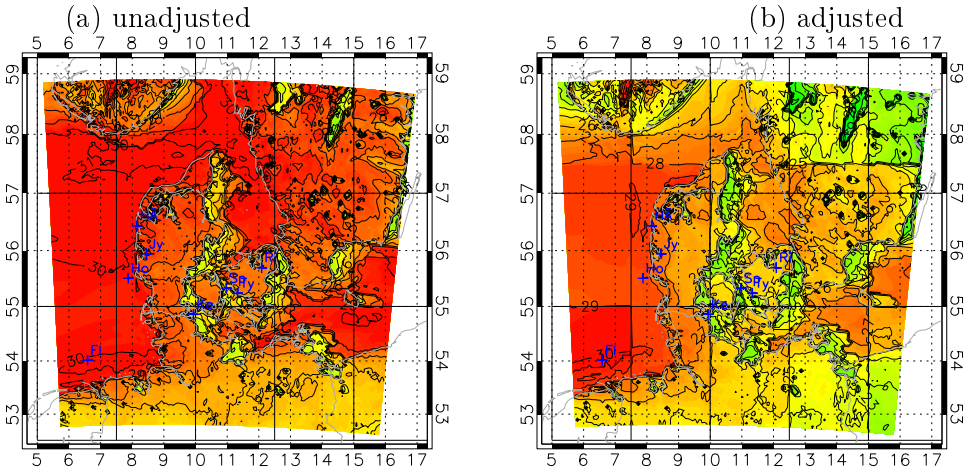

Figure 30: As in Figure 29 except for extreme geostrophic wind cases based on e11n56.

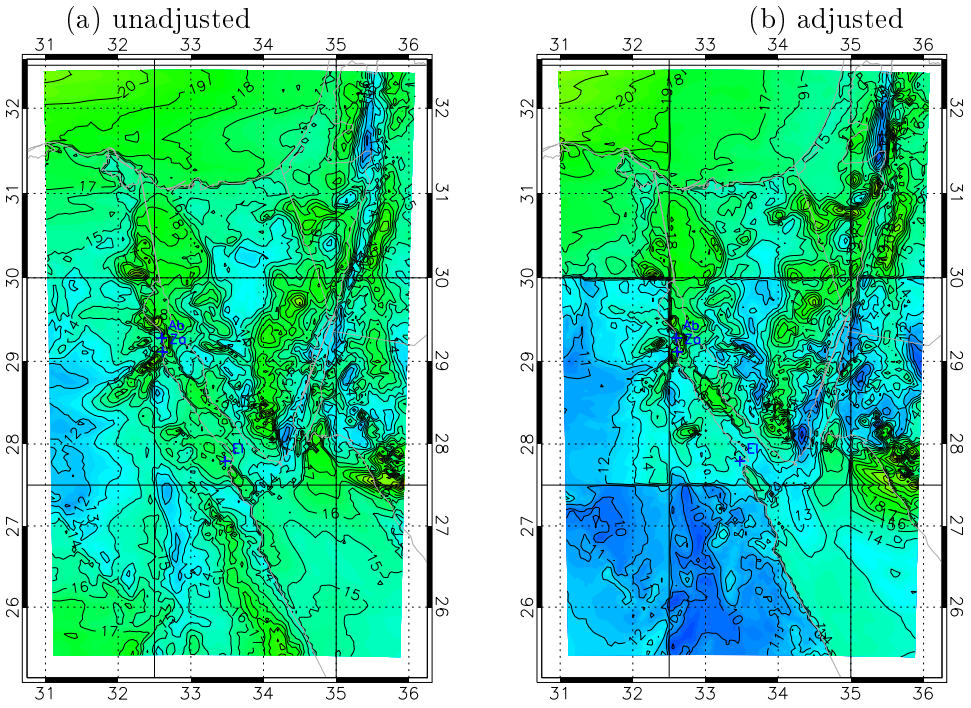

Figure 31: Maps showing the estimated 50-year extreme wind for Gulf of Suez and surroundings at 10 m a.s.l. from (a) the unadjusted methodology and (b) from the adjusted. The extreme wind cases were based on location e33n28 and the water roughness, $z0w = 0.02$ m. The solid grid lines indicate the partions between the reanalysis grid points. The blue annotations indicate the measurement station locations, accompanied by the first two letters of the station name.

Table 6: Table summarizing the performance over Denmark of the statistical downscaling methodology without the adjustment for variation of extreme geostrophic wind cases over the modelling domain; referred to as the unadjusted methodology. The columns give the percentage error for the extreme wind estimate when the i. the simulations use extreme geostrophic wind cases from difference reanalysis grid points and ii. different surface roughnesses are used for water. The table also gives the mean absolute error for different groupings of the measurement stations, i. all stations, ii. only stations over land, and then iii. station inside the closest to the different reanalysis grid points used for the extreme geostrophic wind case definitions.

	z0w=0.0002 m				z0w=0.002 m				z0w=0.02 m			
	e08n56	e06n53	e08n53	e11n56	e08n56	e06n53	e08n53	e11n56	e08n56	e06n53	e08n53	e11n56
Sprogoe	-10.3	-2.27	-4.18	-11	-8.07	-2.41	-1.73	-10.3	-0.77	-0.68	4.11	-5.35
Tystofte	2.9	6.09	4.83	-3.09	2.9	6.09	4.83	-3.09	2.9	6.09	4.83	-3.09
Kegnaes	-15.1	-3.84	-7.89	-15.5	-15.1	-3.83	-7.68	-15.7	-15.5	-3.83	-7.29	-15.7
Jylex	-5.64	5.45	2.02	-8	-5.64	5.45	2.02	-8	-5.64	5.45	2.01	-8
Risoe	4.3	19.8	13.7	4.34	4.3	19.8	13.8	4.34	4.3	19.81	13.71	4.34
Hoevsoere	-14.3	-12.7	-12.3	-15.5	-10.1	-5.87	-6.12	-11.5	0.14	6.59	4.21	-2.83
Horns Rev	-25.2	-18.6	-21.5	-26.6	-20.4	-12.8	-15.9	-21.7	-10.8	-2.98	-6.43	-12.2
FINO1	-22	-14.4	-16.6	-23.8	-16.5	-8.27	-10.6	-18.4	-7.15	2.03	-0.55	-9.32
	mean absolute error											
all	12.47	10.39	10.38	13.48	10.38	8.07	7.84	11.63	5.9	5.93	5.39	7.6
land only	6.99	8.8	7.11	7.73	6.99	8.79	7.08	7.78	7.09	8.8	6.96	7.78
08n56	15.05	12.25	11.94	16.7	12.05	8.04	8.01	13.73	5.53	5.01	4.22	7.68
06n53	22	14.4	16.6	23.8	16.5	8.27	10.6	18.4	7.15	2.03	0.55	9.32
08n53	15.1	3.84	7.89	15.5	15.1	3.83	7.68	15.7	15.5	3.83	7.29	15.7
11n56	5.83	9.39	7.57	6.14	5.09	9.43	6.79	5.91	2.66	8.86	7.55	4.26

Table 7: Table summarizing the performance over Denmark of the statistical downscaling methodology with the adjustment for variation of extreme geostrophic wind cases over the modelling domain; referred to as the adjusted methodology. The structure of the table is otherwise the same as in 6.

	z0w=0.0002 m				z0w=0.002				z0w=0.02			
	e08n56	e06n53	e08n53	e11n56	e08n56	e06n53	e08n53	e11n56	e08n56	e06n53	e08n53	e11n56
Sprogoe	-12.4	-9.53	-9.37	-12.5	-11	-8.13	-7.95	-10.6	-7.6	-4.58	-3.46	-5.59
Tystofte	-2.83	0.09	-2.55	-4.26	-2.83	0.09	-2.55	-4.26	-2.83	0.09	-2.55	-4.26
Kegnaes	-12.9	-10.3	-11.6	-13.1	-12.6	-10.1	-11.3	-12.3	-12.2	-9.51	-10.8	-11.2
Jylex	-6.4	-1.53	-2.14	-6.09	-6.4	-1.53	-2.14	-6.09	-6.4	-1.53	-2.14	-6.09
Risoe	2.59	8.05	6.55	3.44	2.59	8.05	6.55	3.44	2.59	8.05	6.55	3.44
Hoevsoere	-17.6	-14.5	-14.6	18.1	-13.1	-10.5	-10.1	-14.2	-4.98	-2.12	-0.31	-5.86
Horns Rev	-26.3	-23.7	-24.1	-26.4	-21.5	-18.3	-19.1	-21.3	-12.9	-9.23	-10.1	-12.3
FINO1	-18.5	-16.7	-16.3	-18.4	-12.7	-10.7	10.35	-12.6	-2.91	-0.75	-0.32	-2.86
	mean absolute error											
all	12.44	10.31	10.3	11.66	9.66	8.43	9.04	9.39	6.28	4.43	4.85	6.45
land only	6.18	4.99	5.71	6.72	6.11	4.94	5.64	6.52	6.01	4.8	5.51	6.25
e08n56	16.77	13.24	13.61	16.86	13.67	10.11	10.45	13.86	8.09	4.29	4.18	8.08
e06n53	18.5	16.7	16.3	18.4	12.7	10.7	12.6	2.91	0.75	0.32	2.86	2.86
e08n53	12.9	10.3	11.6	13.1	12.6	10.1	11.3	12.3	12.2	9.51	10.8	11.2
e11n56	5.94	5.25	4.56	3.72	3.67	5.42	5.68	6.1	4.34	4.24	4.19	4.43

Table 8: Table summarizing the performance over Gulf of Suez of the statistical downscaling methodology without the adjustment for variation of extreme geostrophic wind cases over the modelling domain; referred to as the unadjusted methodology. The columns give the percentage error for the extreme wind estimate when it is based on i. the single nearest grid point to the measurement station, the mean of the 9 grid points centered at the station or the maximum of the 9 grid points centered at the station, and ii. different surface roughnesses are used for water. The table also give the mean absolute error.

	e33n28								
	z0w=0.0002 m			z0w=0.002 m			z0w=0.02 m		
	nearest	mean	max	nearest	mean	max	nearest	mean	max
AbuDarag	-23.2	-23.9	-18.5	-23.2	-21.6	-15.2	-23.2	-17.8	-4.00
Zafarana	-6.50	-11.0	1.98	-6.50	-11.0	1.98	-6.50	-11.0	1.98
El-Zayt	-3.88	-3.05	-0.22	-3.90	-3.06	-0.22	-3.88	-3.10	-0.22
	mean absolute error								
all	11.2	12.7	6.90	11.2	11.9	5.80	11.2	10.6	2.07

Table 9: Table summarizing the performance over Gulf of Suez of the statistical downscaling methodology with the adjustment for variation of extreme geostrophic wind cases over the modelling domain; referred to as the adjusted methodology. The structure of the table is otherwise the same as in 8

	e33n28								
	z0w=0.0002 m			z0w=0.002 m			z0w=0.02 m		
	nearest	mean	max	nearest	mean	max	nearest	mean	max
AbuDarag	-24.0	-25.0	-18.7	-24.0	-22.9	-15.4	-24.0	-19.3	-4.58
Zafarana	-7.06	-11.4	1.35	-7.06	-11.4	1.35	-7.06	-11.4	1.35
El-Zayt	-21.8	-20.6	-19.2	-21.8	-20.6	-19.2	-21.8	-20.7	-19.2
	mean absolute error								
all	17.6	18.7	13.3	11.7	18.3	12.0	17.6	11.3	8.38

9.2.1 Denmark study

For the unadjusted methodology the mean absolute error (MAE) ranges from 10.4 % to 12.5 % for the $z0w = 0.0002$ m cases depending on which location is used for the geostrophic extreme wind case definitions. This error has a large contribution from the offshore sites, the land-only sites have a MAE ranging from 7.0 % to 8.8 %. This error offshore has been addressed by altering the water roughness used in the generalization process. Roughness length values of $z0w = 0.002$ m and $z0w = 0.02$ m were also used. The land sites are little affected by these changes, but the estimates for the offshore sites are improved. For $z0w = 0.002$ m, the all sites MAE ranges from 7.8 % to 11.6 % and for $z0w = 0.02$ m, the all sites MAE ranges from 5.4 % to 7.6 %.

Now consideration is given to which location's set of extreme geostrophic wind cases gives the best results. Considering only the land sites first, the best estimates, with MAE of 7.0% are achieved by sets using e08n56n and e08n53 extreme geostrophic wind cases. And this is irrespective of the roughness given to water in the generalization process.

Considering all sites, the best estimates, with MAE of 5.4% are achieved by using e08n53 extreme geostrophic wind cases, and $z0w =$ 0.02 m.

It may be hypothesized that the best estimates are obtained by using the extreme geostrophic wind cases defined at the closest reanalysis point for each of the measurement stations. The sample size is rather small, when sites are grouped according to nearest reanalysis grid points, and perhaps for this reason the hypothesis cannot be shown to be true. However the worst estimate is never obtained from the extreme geostrophic wind cases defined at the closest reanalysis point. In fact it is the 2nd best estimate in 3 cases (e06n53, e08n43, e11n56) and the 3rd best in 1 case (e08n56).

This may indicate that the spread of the estimates is only partly due to the variation in the extreme geostrophic wind cases across the domain, and other uncertainties are introduced, for example in the Gumbel fitting, which plays just as an important role. As described earlier, an adjustment methodology has been designed within the methodology from the outset, as a way to reduce uncertainty. Next the results obtained with the inclusion of the adjustment in the methodology are examined.

For the adjusted methodology the mean absolute error (MAE) ranges from 10.3 % to 12.4 % for the $z0w = 0.0002$ m cases. This is very similar to the unadjusted methodology cases. The land only sites have a MAE ranging from 5.0 % to 6.7 %, this is a little lower than in the unadjusted methodology cases. Altering the water roughness used in the generalization process, as before improved the estimates for the offshore sites. Using $z0w = 0.002$ m the all sites MAE ranges from 8.3 % to 9.7 % and for $z0w = 0.02$ m, the MAE ranges from 4.3 % to 6.5 %. These last values indicate a slight improvement compared to the unadjusted MAE for the same cases.

Considering all sites, the best estimates, with MAE of 4.4% are achieved by using e08n53 extreme geostrophic wind cases, and $z0w =$

0.02 m, (c.f 5.4% when using the unadjusted methodology). Considering only the land sites, the same case gives best estimates, with MAE of 4.8% (c.f 7.0% when using the unadjusted methodology).

9.2.2 Gulf of Suez study

For the Gulf of Suez study the measurement stations are located with a relatively small area compared to the of a reanalysis grid point. The nearest mid-grid point is the same for all the stations (e33n28). Therefore the verification is a little different in form compared to the verification for the Denmark study.

Table 8 summaries the verification for the unadjusted methodology, which uses the generalized mesoscale surface winds more directly in the analysis, the mean absolute error (MAE) with water roughness $z0w = 0.0002$ m is 11.2 %. The errors are are unestimations of the extreme wind at all three stations. All of the sites are on land, therefore altering the water roughness in the generalization step has no impact, as can be seen in the table. One possible reason for the error is the choice of mesoscale grid point used to represent the station location. Instead of choosing a single mesoscale grid point, the mean of the nearest point, and the surrounding eight grid points tested. When the mean of the nearest grid points is used, the MAE goes up slightly to 12.7 %. This indicates that the result is not due to anomolous single nearest grid points. Finally the maximum estimate of the extreme wind from the nearest and surrounding eight grid points is tested. When the maximum estimate is used, the MAE goes down to 6.9 %. This suggests that the stations are located in areas where there is a rapid change in the extreme wind climate when moving just a few kilometers from the station. This effect becomes more pronounced for the Abu Darag station when the water roughness is increased, to $z0w = 0.002$ m and $z0w = 0.02$ m. In this case a grid point close to or over water is acting to increase the maximum estimate of the extreme wind. Using the water roughness $z0w = 0.02$ m and the maximum estimate from surrounding eight grid points achieves a MAE = 2.07 %

Table 9 summaries the verification for the adjusted methodology for the Gulf of Suez. This is presented for completeness, because in fact all the stations have as there nearest reanalysis mid-grid point e33n28 which is also the location used to define the extreme geostrophic wind cases for the modelling. Therefore the adjustment methodology is not necessary and would be expected to give poorer results, due to the limitation of the empirical drag law, as was seen for the Denmark study. Using $z0w = 0.0002$ m and taking the nearest mesoscale grid point estimate gives a MAE = 17.6 %. As anticipated this is a poorer performance than the unadjusted methodology. It is particularly poor for the El-Zayt station. This indicates that empirical geostrophic drag law function is giving large uncertainty for this location. The error at El-Zayt is -21.6 % using the adjusted methodology, compared to -3.88 % for the unadjusted methodology. Using the maximum estimate from the surrounding mesoscale grid points reduces the MAE to 13.3

%. Furthermore, increasing the water roughness, once again has a benefitial impact on the estimate of the Abu Darag extreme wind; reducing MAE from -18.7 % to -4.58 %, when the maximum estimate is used. Overall, using the water roughness $z0w$ = 0.02 m and the maximum estimate from surrounding eight grid points achieves a MAE = 8.38 %. This is markedly higher error compared to the unadjusted methodology (MAE = 2.07 %).

9.2.3 Discussion: Empirical geostrophic drag law

In the previous section, it was seen that the adjusted methodology had a poorer performance for the El-Zayt measurement station, whereas, particularly for the Denmark study measurement stations the performance of the adjusted methodology was good. In this subsection the sectorwise characteristics of the linear regression used determine the empirical geostrophic drag law are investigated for a single Denmark study measurement station and the three Gulf of Suez study measurement stations. The sector is defined by the direction of the extreme geostrophic wind case forcing.

Tables 10 and 11 present the main sectorwise characteristics. For the Denmark station, Kegnaes, it is seen that the multilinear correlation coefficient (with reference to the input variables and output variable of Eq. 10) ranges from 0.80 to 0.96 across the 12 direction sectors. For the Gulf of Suez stations the multilinear correlation coefficient ranges are 0.38 to 0.97 for Abu Darag, 0.34 to 0.97 for Zafarana, and 0.13 to 0.96 for El Zayt. From the lower limit of the ranges it can seen that El Zayt has a sector where the linear function of Eq. 10 provides a poor fit. Further it can be seen that this poorly fitted geostrophic wind sector (sector 2) is one with the largest mean for the generalized mesoscale 10 m a.s.l wind, suggesting it may be important in determining the extreme mesoscale winds. This is confirmed by inspection of Figure 33 to be introduced in the next section.

It is also interesting to check the standard deviations of the generalized mesoscale 10 m a.s.l wind and the output of the fitted function (Eq. 10). In a good fit the standard deviations would be comparable. This is mainly the case for the Denmark station, Kegnæs. Here there is a small and systematic tendency to underestimate the standard deviation of the generalized mesoscale 10 m a.s.l winds. For the Gulf of Suez stations, the fitted function also always underestimates the standard deviation of the generalized mesoscale 10 m a.s.l winds, but in some sectors there is a gross underestimation. Again it is El Zayt and sector 2 that demonstrates a particularly drastic underestimate of the standard deviation. The underestimation of the standard deviation of the generalized mesoscale 10 m a.s.l winds is associated with a narrower distribution with fewer and weaker extremes, which is likely to impact the annual maximum method result by giving a underestimate of the 50-year wind.

Table 10: Table giving for a Denmark station, Kegnæs, characteristics of the fitted linear regression used to create the empirical geostrophic drag law employed in the adjusted methodology. The data is for extreme geostrophic wind cases defined at e08n53.

		sector number											
station	quantity	1	2	3	4	5	6	7	8	9	10	11	12
Kegnaes	mean	9.84	7.94	7.68	10.01	11.24	10.05	9.14	10.91	15.12	16.41	15.85	13.60
	model st. dev.	2.22	1.77	1.19	1.68	1.94	1.58	1.18	1.77	2.05	2.54	2.98	2.31
	fit st. dev.	1.80	1.67	1.10	1.44	1.86	1.27	1.06	1.60	1.94	2.24	2.78	2.09
	correl.	0.81	0.94	0.93	0.85	0.96	0.80	0.90	0.90	0.94	0.88	0.93	0.91

Table 11: Table giving for the Gulf of Suez stations the characteristics of the fitted linear regression used to create the empirical geostrophic drag law employed in the adjusted methodology. The data is for extreme geostrophic wind cases defined at e33n28.

		sector number											
station	quantity	1	2	3	4	5	6	7	8	9	10	11	12
AbuDarag	mean	8.73	11.05	11.12	8.72	3.80	7.74	10.98	9.82	5.53	5.42	4.92	7.06
	model st. dev.	1.18	0.80	1.41	1.12	1.95	2.40	2.20	2.16	1.75	1.70	2.90	1.82
	fit st. dev.	0.95	0.51	0.76	0.48	0.91	1.88	2.13	1.52	0.67	0.87	1.68	1.01
	correl.	0.80	0.63	0.54	0.43	0.46	0.79	0.97	0.71	0.38	0.51	0.58	0.56
Zafarana	mean	8.35	10.75	10.65	8.32	5.02	9.78	12.47	10.62	5.51	5.79	7.07	7.02
	model st. dev.	1.27	0.63	1.11	1.05	2.57	2.53	2.53	2.76	2.07	1.99	2.10	1.65
	fit st. dev.	0.78	0.51	0.74	0.52	0.87	2.18	2.45	2.05	1.00	0.91	1.34	1.26
	correl.	0.61	0.80	0.67	0.49	0.34	0.86	0.97	0.74	0.48	0.46	0.64	0.76
El-Zayt	mean	10.19	12.82	11.78	5.23	5.30	7.16	8.41	6.80	3.72	4.62	6.93	8.74
	model st. dev.	1.36	1.54	2.17	1.77	1.53	1.48	1.84	1.66	1.64	2.41	2.19	1.42
	fit st. dev.	0.90	0.20	0.80	0.89	0.52	1.29	1.78	1.24	1.08	1.42	0.98	1.13
	correl.	0.66	0.13	0.37	0.50	0.34	0.87	0.96	0.75	0.66	0.59	0.45	0.80

9.2.4 Discussion: Sectorwise extreme wind climates

Figures 32 and 33 show for Denmark and Gulf of Suez respectively, for each measurement station the generalized mesocale 10 m a.s.l. wind speed and direction that comprise of the 30 omnidirectional annual maximum wind speeds used in the annual maximum method. The figures also show the 30 extreme geostrophic wind cases that correspond to the maximum mesoscale winds for each station. It is important to note that the 30 extreme geostrophic wind cases are not the omnidirection annual maximum geostrophic winds. This can be seen from the figures by comparing extreme geostrophic wind cases across different stations. Although some extreme gesotrophic wind cases are seen across several stations, the same set of cases are not duplicated across stations. This effect demonstrates the importance of mesoscale impacts on the wind flow. A single extreme case at the large scale does not necessarily mean an extreme at the mesoscale, as it depends on the situation of the station with regard to roughness and orographic terrain features.

For the Denmark stations (Fig. 32) it is notable that the extreme mesoscale winds come from a rather broad range of directions, mainly with a positive westerly component. For the Gulf of Suez stations (Fig. 33) it is notable that the extreme mesoscale winds come from a very narrow range of directions. For Abu Darag and Zafarana a narrow range of northerly (north-north-west) and a narrow range of southerly (south-south-east) directions are prevailent as the extreme wind directions. For El-Zayt the predominatent direction is northwesterly, with a single southeasterly case. What is also remarkable is that the extreme geostrophic wind cases that are associated with the extreme mesoscale winds have a considerably broader direction distribution. This illustrates the channelling effect of the physical geography of the region.

The characteristic of the directional distribution of the extreme mesocale winds has implications for trying to make a sectorwise estimate of the extreme winds. One suggestion for a method to do this would be to partition the mesoscale winds into direction sectors, then carry out the annual maximum method. However a problem must be anticipated in that each sector may not have so many extreme winds populating it. Within the present method, 30 extreme geostrophic wind cases are determined for each sector, but the the eventual direction distribution from the mesoscale simulations can be distributed quite differently. This difficulty is particulary serious in channelling flow cases such as the Gulf of Suez.

9.3 Comparison of results from the two methods

Tables 12 and 13 show the summary of results for the stations in the Denmark and Gulf of Suez studies using the two methodologies described in this report. The tables also give the mean error (bias) and mean absolute error for the estimates. The comparison is made by of comparing generalized 50-year extreme winds at 10 m a.s.l. for flat terrain with 5 cm roughness.

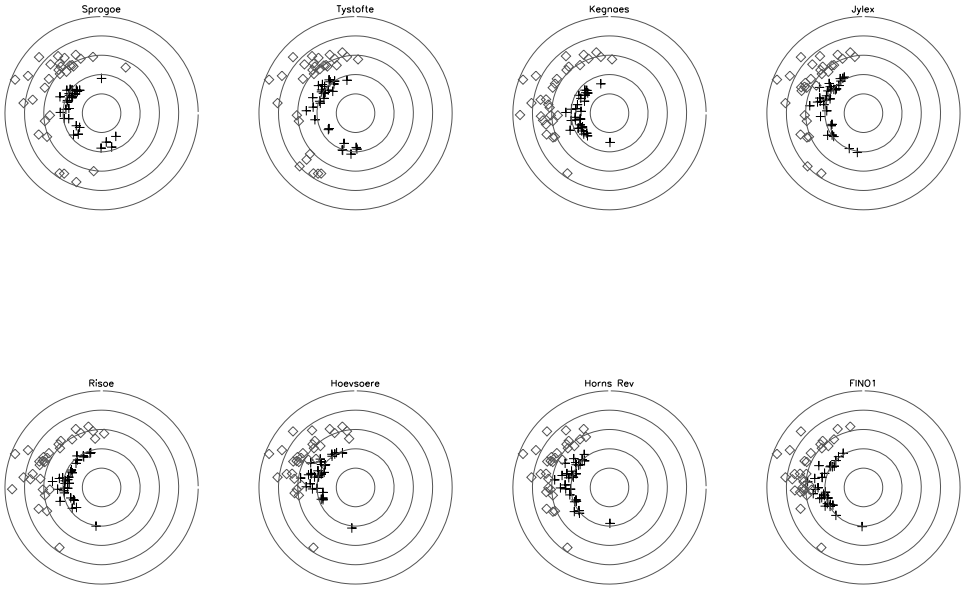

Figure 32: Figures showing the 30 omnidirectional annual maximum 10 m a.s.l generalized mesoscale wind speed and direction (bold + symbols) and their corresponding extreme geostrophic wind case forcing speed and direction (grey diamonds) for the eight measurement stations for the Denmark study. It is these 10 m a.s.l generalized mesoscale annual maximum wind speeds that are fitted to the Gumbel distribution to give the estimate of the extreme winds for each station. The extreme geostrophic wind cases were defined at e08n56 and water roughness $z0w = 0.02$ m is used.

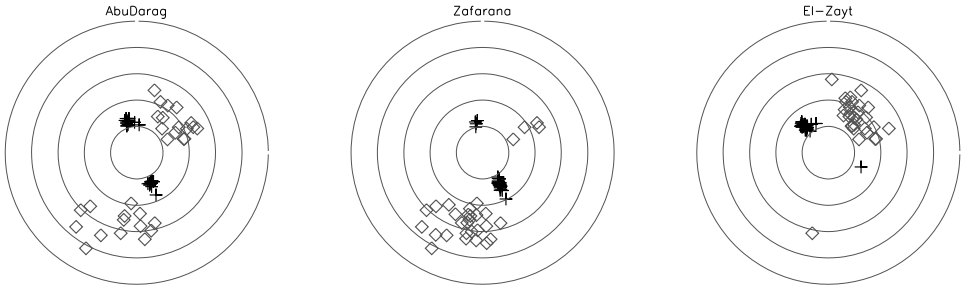

Figure 33: Figures as in 32 but for the three measurement stations for the Gulf of Suez study. The extreme geostrophic wind cases were defined at e33n28 and water roughness $z0w = 0.02$ m is used.

For the Denmark study, the selective dynamical downscaling gives a bias of -1.8 % on the extreme wind and a mean absolute error (MAE) of 4.2 %. For 6 of the 8 stations there is an underestimate of the extreme wind. The largest errors are for Risøÿ (8% overestimate) and Horns Rev (8% underestimate).

The statistical-dynamical downscaling gives a bias of -3.3 % and a MAE of 4.9 %. For 7 of the 8 stations there is an underestimate of the extreme wind. The largest errors are for Kegnaes (10 % underestimate) and Horns Rev (10 % underestimate).

The performance of the two methodologies is very similar. Considering the uncertainty on the measurement based extreme winds, it is fair to describe the agreement of the modelling and observation as good.

For the Gulf of Suez study, the selective dynamical downscaling gives a bias of -3.5 % on the extreme wind and a mean absolute error (MAE) of 4.4 %. For 2 of the 3 stations there is an overestimate of the extreme wind. The largest error is for El-Zayt (11% underestimate).

The statistical-dynamical downscaling gives a bias of -7.2 % and a MAE of 7.5 %. For all stations there is an underestimate of the extreme wind. The largest error is for Abu Darag (-23 % underestimate).

Of the two methodologies, the selective dynamical downscaling performs best for the Gulf of Suez. Considering the uncertainty on the measurement based extreme winds, it is fair to describe the agreement of the selective dynamical downscaling and observation as good. The statistical-dynamical downscaling method has difficulty estimating the Abu Darag extreme wind. The difficult appears to be associated with a strong horizontal gradient of the extreme wind values, i.e. moving to a neighboring mesoscale grid point greatly reduces the error. A possible reason why the WRF model is better at estimating El-Zayt's extreme wind is that the WRF tends to be more diffusive than KAMM, and hence strong horizontal gradients of wind speed do not appear so readily.

The statistical-dynamical downscaling methodology is less computational demanding than the selective dynamical methodology. However, it is expected the the statistical-dynamical methodology will miss extreme winds that are caused by small scale and transient features. This is because of the way the mesoscale model for each simulation is forced with a uniform (no small scale features) and steady (no transient features) large scale geostrophic wind. This disadvantage may result in a underestimate of the extreme winds, but whether it is cause of larger negative bias of the statistical-dynamical methodology compared to the selective dynamical methodology (Tables 12 and 13) is difficult to say.

An advantage of the statistical-dynamical methodology is that the large scale annual maximum wind speeds are determined on a sector by sector basis. This can be important if specific mesoscale effects at specific mesoscale grid points give stronger wind enhancement for particular sectors. This effect was seen to be important in Figures 32 and 33. This possible weakness of the selective dynamical methodology

has been guarded against in this study for the measurement stations, as the wind data at the measurement sites is used to validate the choice of episodes, based on the large scale reanalysis data. However, for any other sites, where no measurement data is available, this safe guarding is not possible. On the other hand, it is possible to modify the episode selection procedure to check for annual maximum in each sector. It is rather likely that the same storm episodes may be responsible for annual maximum over a wide range of directions, and therefore sectors.

Table 12: Table summarizing the Denmark stations estimates of the generalized 50-year extreme wind ($U_{50,st}$) at 10 m a.s.l. for flat conditions with uniform roughness of 5 cm. The estimated error associated with the fit of the Gumbel distribution is given (1.96σ). The estimates are derived from measurements, the selective downscaling method, and the statistical-dynamical downscaling method. Overall mean error and mean absolute error are given at the bottom of the table for the two modelling methodologies.

	OBS		Sel. Dyn.				Stat. Dyn.			
station	$U_{50,st}$	1.96σ	$U_{50,st}$	1.96σ	%error	% abs error	$U_{50,st}$	1.96σ	% error	% abs error
Sprogoe	23.9	2.0	24.2	4.4	1.3	1.3	23.1	3.7	-3.5	3.5
Tystofte	25.7	2.9	25.0	5.4	-2.7	2.7	25.0	4.0	-2.5	2.5
Kegnaes	26.3	3.8	25.8	5.5	-1.9	1.9	23.4	4.0	-10.8	10.8
Jylex	29.1	2.9	27.4	5.4	-5.8	5.8	28.5	4.8	-2.1	2.1
Risoe	23.7	4.7	25.6	5.3	8.0	8.0	25.3	4.3	6.6	6.6
Hoevsoere	29.8	9.4	29.7	5.8	-0.3	0.3	28.8	4.9	-3.3	3.3
Horns Rev	31.6	8.5	29.0	5.3	-8.2	8.2	28.4	4.6	-10.1	10.1
FINO1	30.3	7.6	28.8	4.3	-5.0	5.0	30.2	5.3	-0.3	0.3
mean					-1.8	4.2			-3.3	4.9

Table 13: Table summarizing the Gulf of Suez stations estimates of the generalized 50-year extreme wind ($U_{50,st}$) at 10 m a.s.l. for flat conditions with uniform roughness of 5 cm. The estimated error associated with the fit of the Gumbel distribution is given (1.96σ). The estimates are derived from measurements, the selective downscaling method, and the statistical-dynamical downscaling method. Overall mean error and mean absolute error are given at the bottom of the table for the two modelling methodologies.

	OBS		Sel. Dyn.				Stat. Dyn.			
station	$U_{50,st}$	1.96σ	$U_{50,st}$	1.96σ	% error	% abs error	$U_{50,st}$	1.96σ	% error	% abs error
AbuDarag	20.2	3.4	20.5	4.8	1.5	1.5	15.5	2.0	-23.2	23.2
Zafarana	19.8	2.8	19.9	4.1	0.5	0.5	18.5	3.3	-6.5	6.5
El-Zayt	17.4	2.6	15.5	1.9	-10.9	10.9	16.7	2.1	-3.9	3.9
mean					-3.5	4.4			-7.2	7.5

10 Complex issues in complex terrains - Navara region

The maps of the 50-year wind at 10 m and the generalized 50-year wind in this region are shown in Figure 34.

Many things become complicated in complex terrain areas. The capability of models, mesoscale and microscale, are questioned in dealing with the possible discontinuity of flow caused by steep terrains. Figure 35 shows pictures of the terrain around four sites from Navara covering a range of RIX. Measurements are needed but only measurements are not enough to validate the outputs from models; a convincing approach to make the validation is also needed. It is nothing trivial to make such validations in complex terrains. For the Navara region in particular, [37] followed the concept of [38] to validate their mean wind output from the WRF model at the regional scale. This means the wind fields are "upscaled" to represent an average wind state for a large area, instead of making comparisons between the point measurements and model output for a certain grid box. The argument behind the upscaling is similar to what we mentioned at the end of Section 6.3, namely to reduce the difference of the surface condition between the modeled and measured data. [37] also recommends the regionalized winds because of the possible "representativeness error" of the grid that is closest to the measurement site. This error is caused by the model spatial discretization that smoothes the complexity of surface physical properties such as oropgraphy. This was argued in [37] to lead to a situation in which the simulated volume that includes the actual location of the observational site may not be the most suitable one to represent the observational variability. As a result, they commented that a nearby volume can sometimes better represent the site condition. This however sounds rather empirical and quite difficult to put into practice.

As explained in Section 6.3, a benefit of the post-processing procedure is that it provides a platform where the measured and modeled winds can be compared fairly, when both are converted to similar surface conditions. For the conversion, we use the linear model LINCOM. Complex terrains like in the Navara region, shown as some of the examples in Figure 35, are very challenging for linear models. Often, RIX is used as a measure for the terrain complexity. As shown in Table 14, here only 4 out of 11 sites whose RIX are within the "secure" range (see the discussions at the end of Section 6.3). The site Tudela should be the flattest according to its RIX (= 0), however, looking at the map (Figure 35c), it is only flat a couple of kilometers around. Considering mesoscale flows, it is by no means a simple terrain around this site. Loma Negra is another site with low RIX (= 3.5); however, the picture, Figure 35d, shows that it is right behind a cliff. Even though WAsP has been reported to be able to handle medium complex terrain with RIX up to 20 with some justification, it was considered not adequate for the steep terrains as in many of the sites in the Navara region (N. G. Mortensen from Risø, personal communication). It should be

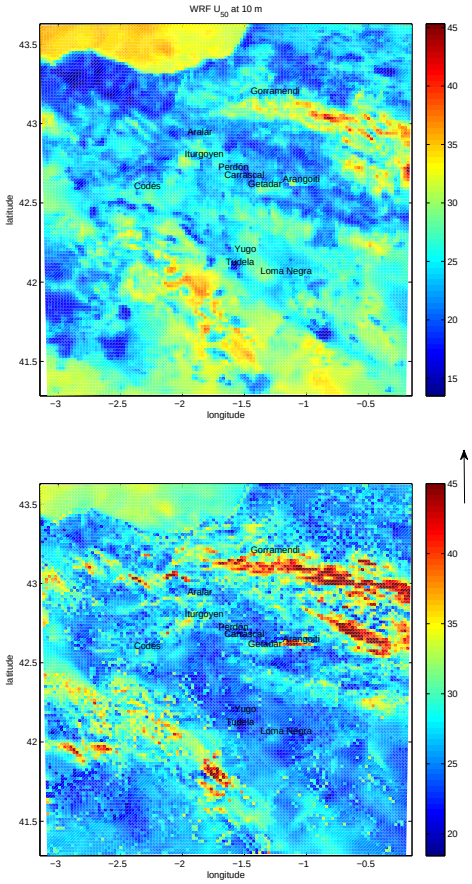

Figure 34: The 50-year wind from the selective dynamical downscaling method. (a): above, at 10 m without post-processing; (b): below, with post-processing.

noted that we obtained the RIX for the Navara sites from CENER and they have used WAsP to calculate RIX over a rather small area around the site. Seemingly, for the measurements in very complex terrains with sharp terrain variation such as cliffs, the WAsP or WEng cleaning procedure is rather limited and is embedded with significant uncertainty. The situation is expected to be different for the mesoscale modeled winds because the complicated microscale topographical and roughness variability are smoothed out. But, it is difficult to conclude exactly to which degree we can trust the modeled results because of the difficulties with using measurements. In the following we validate the model results with different approaches, qualitatively.

For analyzing extreme winds, it is not an optimal approach to upscale the measured winds to regional scale as in [37], firstly because we do not have a large spatial coverage of measurements to give a reasonable average representation of the extreme winds over the area. Secondly, extreme winds are deeply affected by the local effects; it is difficult to say to which degree the upscaled, or in other words, smoothed, extreme winds from a number of sites can represent the average extreme wind over a region like Navara. To take into account of the complexity around the sites, we study the spatial variability of the 50-year wind together with the orography and roughness length. The 50-year winds without post-processing are plotted at the corresponding grid point closest to each of the 11 sites plus a squared area around it including 11 by 11 grid points (the 1st column in Figure 36 and 37). At the same time, the corresponding orography and roughness length as used in the WRF modeling and $U_{50,st}$ in the same area are plotted together (2nd, 3rd and 4th columns, respectively).

Looking at Figures 36 and 37, one understands that the "representativity error" as mentioned in [37] is very easy to happen at many of these sites. There is a considerable gradient of terrain elevation a couple of kilometers around the middle point, which is the grid point (black dot) closest to the site location (red dot) and the distribution of U_{50} at 10 m reflects the terrain variation. Even for the "flattest" Tudela, the change in U_{50} at 10 m can be as large as 16 ms^{-1} within the distance of less than 20 km. At the same time, the changes in the roughness length are very significant. The current codes for the post-processing react quite strongly to the roughness change, leading to significant gradient in $U_{50,st}$ around the sites.

It is clear that further investigation is needed to evaluate the post-processing procedure in the very complex terrains, not only for measurements but also for mesoscale modeled winds.

In the following subsection, we examine the spectral behavior of wind speed in the Navara region and make use of it to correct the extreme winds calculated from two data sets (1) the NRA-2 data using the method described in [10] (Section 2.3); (2) the WRF storm simulations using the selective dynamical method as described in Section 6.

The values of U_{50} at 10 m from measurements are extracted from a figure presented in [23].

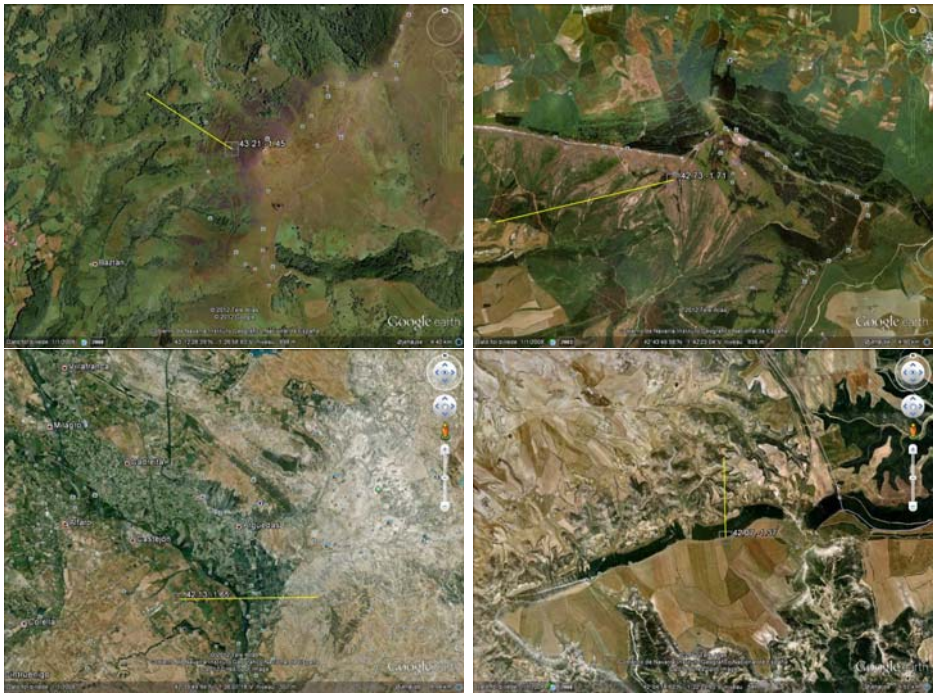

Figure 35: Pictures of several example sites showing the site conditions. (a), upper-left, Gorramendi, at the end of the yellow line to the right. The line shows a distance of 1 km. (b) upper-right, Perdón, at the end of the yellow line to the right. The line shows a distance of 2 km. (c) below-left, Tudela, at the end of the yellow line to the left. The line shows a distance of 10 km. (d) below-right, Loma, at the bottom end of the yellow line, the line shows a distance of 1 km.

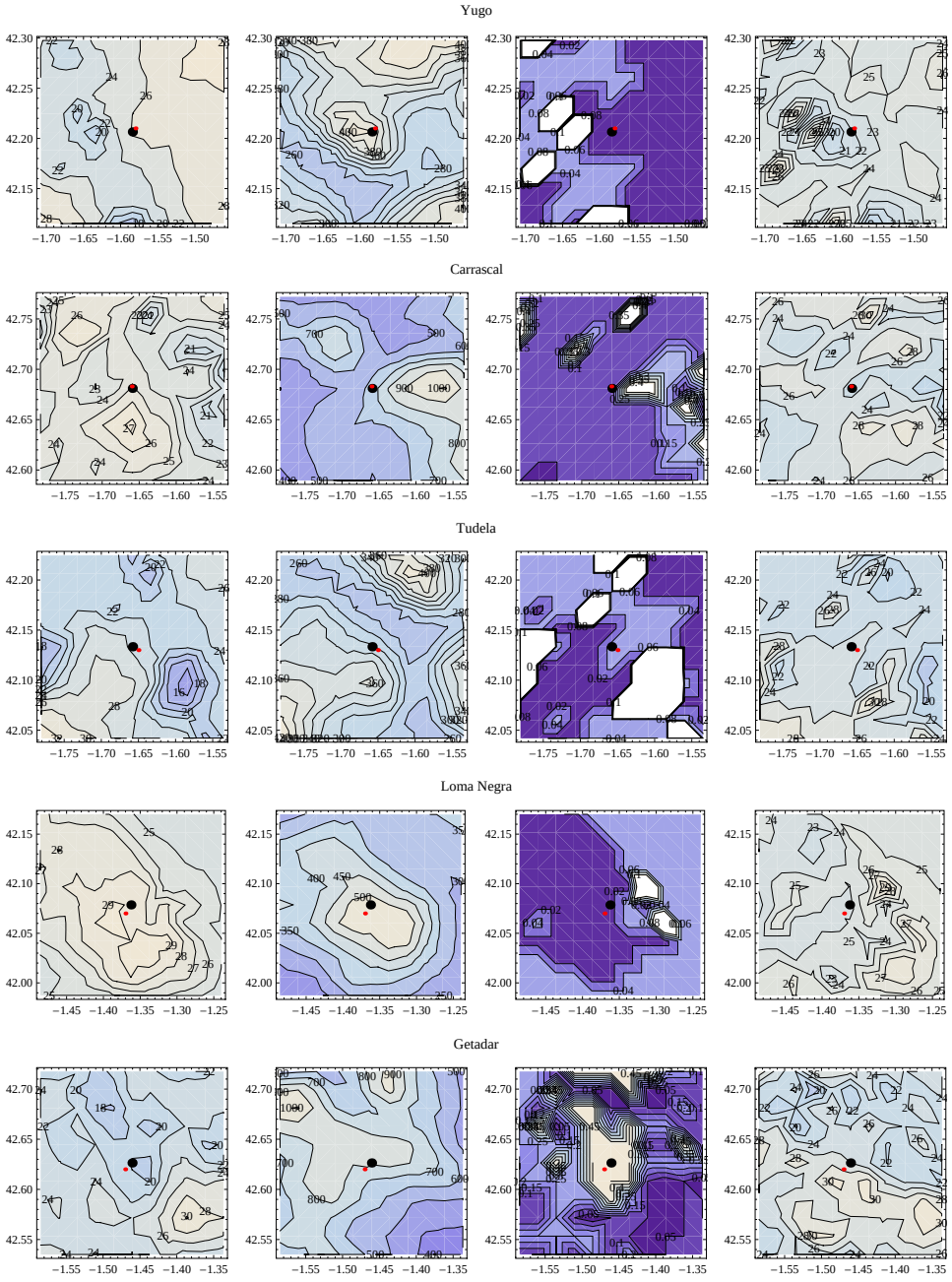

Figure 36: 11 by 11 grid points with the one closest to the site (small red dot) in the middle (big black dot), from left column 1: U_{50} (ms^{-1}) at 10 m; column 2: elevation h (m); column 3: roughness length z_0 (m); column 4: $U_{50,st}$, for 5 of the 11 sites, to be continued in Figure 37.

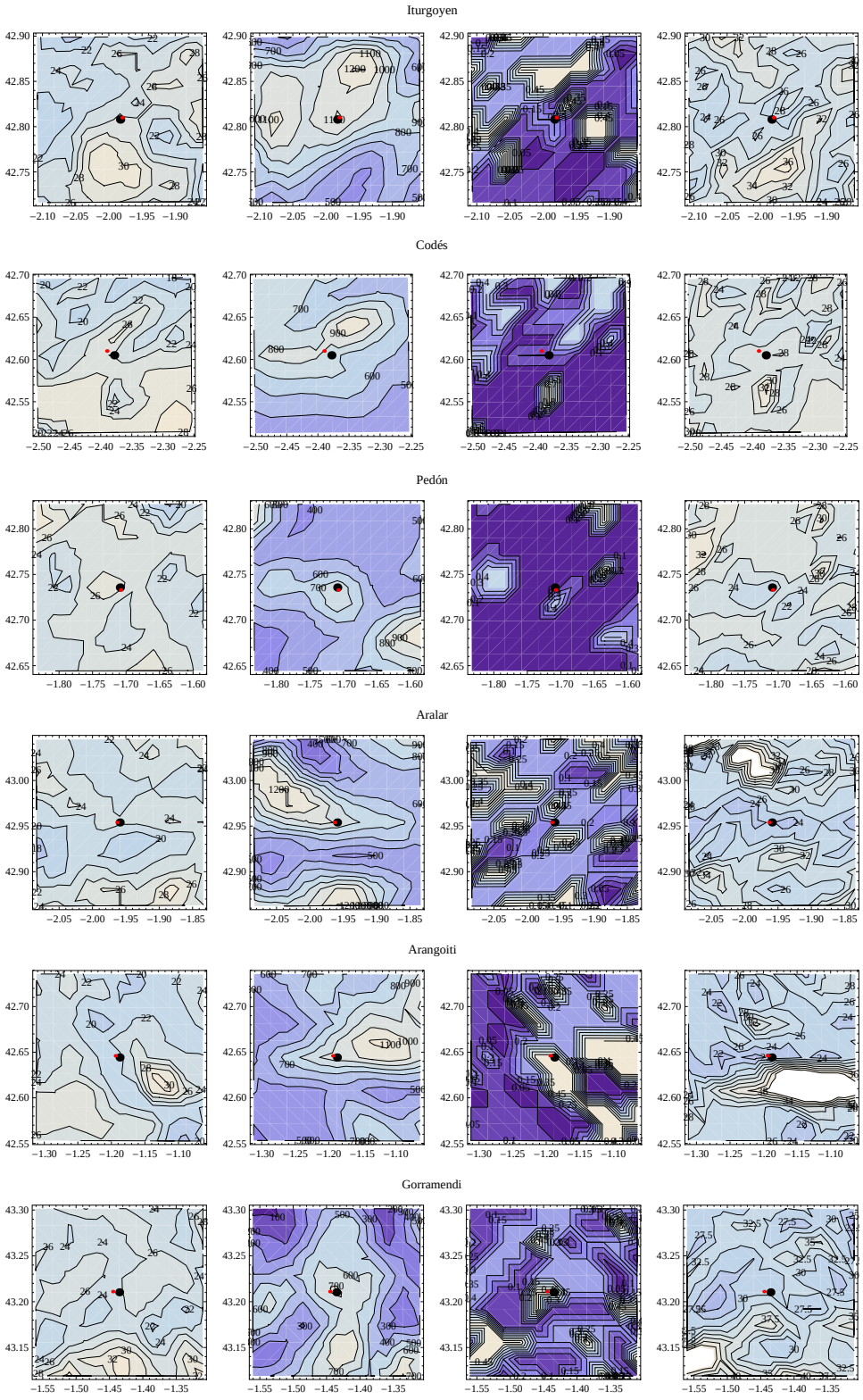

Figure 37: Same to Figure 36 but for 6 other sites.

Table 14: The 50-year wind at 10 m at the sites without post-processing. WRF(a) means outputs from all years from 1999 to 2011 are used. WRF(o) means the WRF output in the overlapping period of measurements are used. The numbers in the parentis have been corrected from the 1 hour values to 10 min values according to [12].

		U_{50}, no generalization		
Stations	RIX	WRF (a)	WRF (o)	OBS
Yugo	0.4	26.2±6.2	24.6±5.6	24 (25.2)
Carrascal	2.6	25.2±5.4	24.8±5.8	25 (26.3)
Tudela	0.0	25.5±6.2	25.5±7.1	18 (18.9)
Loma Negra	3.5	28.9±6.8	26.4±5.2	32 (33.6)
Getadar	6.6	19.8±3.3	19.3±3.3	15 (15.8)
Iturgoyen	6.8	26.5±5.5	27.0±6.8	28 (29.4)
Codés	8.5	23.8±5.2	22.4±5.2	18 (18.9)
Perdón	8.9	26.5±5.6	25.9±5.9	36 (37.8)
Aralar	19.0	22.4±4.1	23.4±6.0	32.5 (34.1)
Arangoiti	26.0	21.4±3.6	20.0±3.4	27.5 (28.9)
Gorramendi	29.0	26.7±5.1	26.5±6.3	45 (47.3)

10.1 Results from spectral correction for complex terrain

The complexity of the sites is reflected in the power spectra of the local wind speed. As found in [35], compared to flat terrains, the wind variability is more significant in complex terrains. Figure 38 shows the spectra at two sites, one representing Navara "simple terrain" (Carrascal) and one representing Navara complex terrain (Gorramendi). In this figure, the gray curve is the power spectrum from the Danish offshore site Horns Rev and the green curve is expression (14). The thin black curves are expression (14) with the coefficients adjusted to the measurements (the red curves). For Gorramendi, $a_1 = 6 \cdot 10^{-4}$ m^{2}s$^{-8/3}$ and $a_2 = 9 \cdot 10^{-11}$ m^{2}s^{-4}. For Carrascal, $a_1 = 5 \cdot 10^{-4}$ m^{2}s$^{-8/3}$ and $a_2 = 3 \cdot 10^{-11}$ m^{2}s^{-4}. In [3] it was shown that long term measurements from 7 sites in Denmark, land and offshore, provide consistent power spectra to that of Horns Rev as in Figure 38. Over flat terrains whereas the climatological spectrum is very simple, the spectrum in the range of our interest here, $10^{-5} < f < 10^{-3}$ Hz, does bare special characteristics for structured meteorological phenomena such as gravity waves and open cells. However, in complex terrain, the wind variability seems to be related to the variability of the orography. Part of the range $10^{-5} < f < 10^{-3}$ Hz seems to be in the sub-mesoscale range, an interface between mesoscales and microscales. It is expected this interface to be somehow different in complex terrain from flat terrain as in Denmark. Here, even the "simple" terrain Carrascal is not actually simple, as can be seen in Figure 36. Seemingly, the RIX numbers provided by [23] have been calculated using a quite small area (a

couple of kilometers) around the site; any mesoscale variability of the terrain has not been taken into account.

The complexity of the sites is also reflected in the integral time scale T. The NRA-2 data suggests $T \sim 0.9$ day, the typical synoptical scale of the atmospheric movement in the region. However, from measurements $T \sim 0.37$ day for Carrascal and $T \sim 0.5$ day for Gorramendi are obtained, strongly suggesting a local variability with smaller scales that is absent in the coarse resolution model data. Note, the 10-min measurements used to calculate T from the two sites are from year 2008.

Seemingly, the power spectrum in the mesoscale range varies with the complexity of the terrain, it is not straightforward how to model it. Obviously the model, expression (14), which was based on flat terrain data, underestimates the variability here (Figure 38). Within this project we have only limited access to the 10-min measured time series through the EU Safewind project: they are from Carrascal and Gorramendi sites for the year 2008. According to [2], the 1-year time series can provide the power spectrum sufficient for the spectral correction and they are used to both the NRA-2 and WRF modeled storm data here.

Figure 40 shows the 50-year wind calculated from the geostrophic wind using the method given in [9, 10] with NRA-2 data. The values in the parentis have been corrected using the spectral approach in [2] for non-measurement situation (Section 8.1); namely expression (14) has been used. This plot shows the 50-year winds caused by the synoptic atmospheric movement when converted to the standard conditions. The wind variation from NRA-2 data in Spain is simple and similarly in the Navara region. The 50-year standard wind strength is about 20 to 22 ms^{-1} in the Navara region, stronger in the north-west part where it is close to the Atlantic Ocean. Compared to Figure 40, we can see that the extreme wind atlas from the selective dynamical method (Figure 34b) adds mesoscale variability reflecting the elevation and roughness length and at the same time $U_{50,st}$ are at a comparable level to that in Figure 40b. Zooming in to the areas of the measurement sites (Figure 36 and 37, 4th columns), we can see that the base 50-year standard wind strength is about 20 to 22 ms^{-1} but the values can be as high as 30 ms^{-1} due to the mesoscale topographical and roughness length effects. Seemingly, even though the spectral correction using flat terrain spectral model adds values to the NRA-2 extreme winds to a comparable level to flat terrain, the extreme winds from the selective dynamical method captured mesoscale variability has reflected more spatial terrain effects.

Figure 39 shows how measurements are used in the spectral correction for NRA-2 extreme winds. Note, automatically, the two sites Carrascal and Gorramendi share the same NRA-2 grid point, which could imply systematic bias due to the missing mesoscale variability. The blue curves with $f > 0.005$ day^{-1} are power spectra from the 1-year 10-min time series. The fluctuations around the low frequency limit of 1 year are simply noises. According to [2], if we start the cor-

rection at $f_c = 1/T$, where $T \sim 0.37$ day at Carrascal and $T \sim 0.5$ day at Gorramendi, the corrected $U_{50,st}$ with an equivalent temporal resolution of 10-min are 28.4 ms^{-1} and 30.9 ms^{-1}. Allowing an uncertainty of T of the order of 0.1 day, $0.27 \leq T \leq 0.47$ day at Carrascal and $0.4 \leq T \leq 0.6$ day at Gorramendi, the range of $U_{50,st}$ becomes $[28.0, 29.2]$ ms^{-1} at Carrascal and [30.1, 31.8] ms^{-1} at Gorramendi. They are considerably greater than using the spectral model for flat terrain. However, it should be noted that here we are combining the spectrum of u_{st} calculated from NRA-2 data with that of the actual wind speed from measurements (u_{10m}), thus having assumed the fluctuation of u_{st} is the same as u_{10m}. In this way we possibly added also the microscale variability embedded in the actual time series to the correction. If so, there must be a slight overestimation of $U_{50,st}$. Further studies are needed to investigate the interface of the mesoscale and microscale interface over different types of terrains.

When applying the selective dynamical method as described in Section 6, we have recorded the outputs on 10-min basis disjunctively. The spectral analysis of the time series of the storm winds together with measurements in flat and medium complex terrains suggested that the variability of the storm winds are reasonably well simulated (e.g. Figure 6 in [1]). This quality of the modeled storm winds in the complex terrain is tested here too.

The spectra of the time series of wind speed during each storm are calculated and averaged for the two sites Carrascal and Gorramendi and they are presented in Figure 41. It is quite clear there misses some energy in the mesoscale modeled wind time series in the high frequency range. For Gorramendi, the energy deficiency starts at about 10^{-4} Hz which corresponds to about 2 hours. For Carrascal, the energy deficit starts at about $1.8 \cdot 10^{-4}$ Hz, which corresponds to one and half hours. The mean wind speed calculated from the 10-min time series is 6 ms^{-1} for Carrascal and 8 ms^{-1} for Gorramendi. The mesoscale modeling misses some of the variability for scales smaller than 2 hours for Gorramendi and misses that for scales smaller than one and half hours for Carrascal. In other words, the flow in WRF was smoothed in the mesoscale modeling within about 60 km around Gorramendi and about 30 km around Carrascal. The comparison of the modeled and measured spectra shows the degree of smoothing, which is obviously more significant at Gorramendi. The impact of the smoothing of the WRF modeled storms in comparison with the measurements is estimated. The smoothing effect is only 2% at Carrascal and 5.5% at Gorramendi, resulting in the final estimation of $U_{50,st}$ from the selective dynamical method for the Carrascal and Gorramendi sites are 23 and 30.9 ms^{-1}. Compared to the method of using G from NRA-2 data with the spectral correction, the selective dynamical method gives show a consistent estimate for Gorramendi but systematically smaller winds at Carrascal. This seems to agree with the measurements better because the winds measured at Gorramendi are significantly greater than Carrascal, even though the local speed up effect could be the major cause.

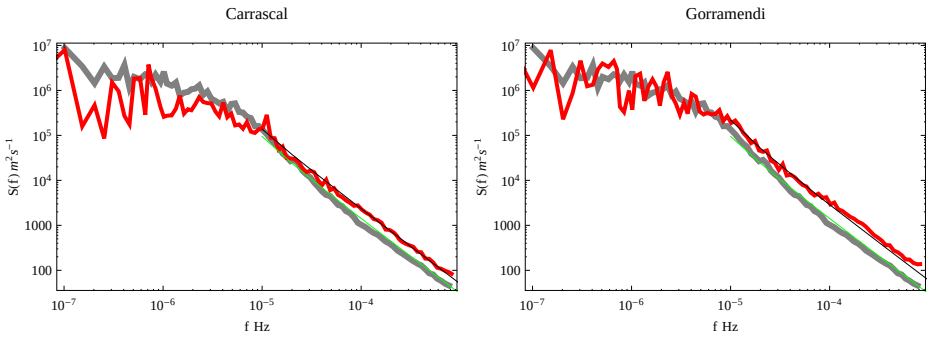

Figure 38: The spectrum of the 10 m winds from Carrascal (left) and Gorramendi (right). The thick gray curve is from the Danish site Horns Rev. The green and black curves are from expression (14) with different coefficients.

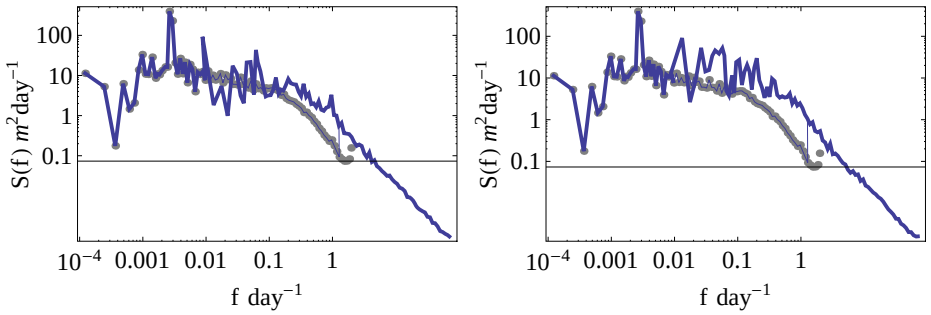

Figure 39: The spectra for the site Carrascal (left) and Gorramendi (right). The spectrum from the NRA-2 data is plotted in gray dots and that from the one-year measurements is plotted in blue.

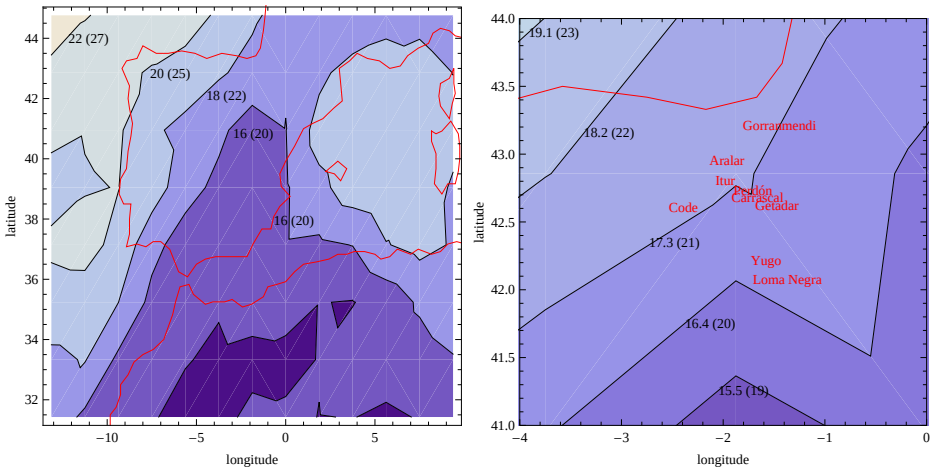

Figure 40: The 50-year standard wind obtained from NRA-2 data over Spain and surroundings (left, the numbers in the parentis are corrected using the spectral correction approach) and over the Navara region (right, not corrected values) where the sites are marked.

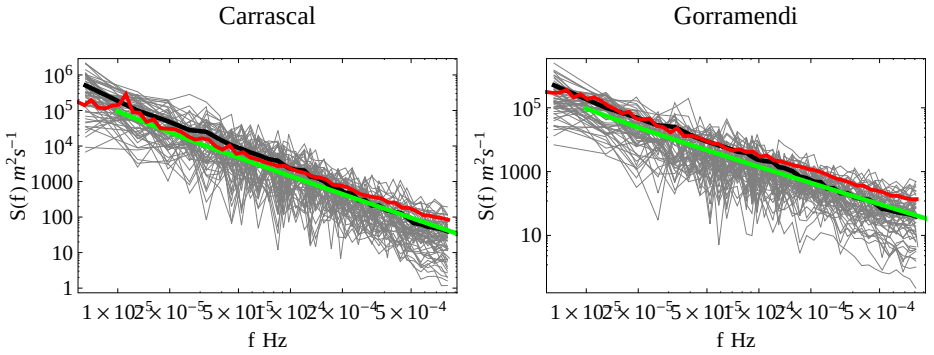

Figure 41: The spectra of the 10 m winds from each WRF modeled storms at the grid point closest to Carrascal (left) and Gorramendi (right), in thin gray lines. The average value of the 62 curves is plotted as the thick black curve. The red curve is from the 1-year 10-min measured time series. The green curve is expression (14) with $a_1 = 3 \cdot 10^{-4}$ and $a_2 = 3 \cdot 10^{-11}$.

11 The statistical distribution for obtaining the 50-year wind

As discussed in [1], the annual maximum method (AMM) is used for obtaining the 50-year wind in the current project. This regards to the two dynamical downscaling methods and the spectral approach described in Section 6, 7 and 8. A Gumbel distribution was applied to the annual maximum winds sorted in ascending order; the algorithms can be found in e.g. [39, 10, 1].

In [3], we extensively examined the uncertainties in the 50-year wind using various distribution functions including the Gumbel distribution to measurements. It was found that the Periodic Maximum Method, including AMM, provides consistent estimates of the 50-year wind to the Peak-Over-Threshold method (also called independent-storm method), according to the measurements from Denmark. Here, the shape parameter as in the distribution functions is found to be close to zero, which supports our choice of using Gumbel distribution. The annual maximum wind distribution from the WRF modeled wind shows the consistent quality on the close to zero shape factor.

The sensitivity of the data length on the estimation of the 50-year wind was examined in details in [3] and in [1], it was found that the uncertainty introduced by using 12 years of data is rather acceptable in comparison with the estimates made with 16 years and 28 years of data. This suggests that the 12 to 13 years of simulated storms are reasonably long for the estimation of the 50-year wind.

12 Future developing directions

The methods developed within this project are (among) the most advanced methods for extreme wind estimations. They can be applied to big areas (the selective dynamical downscaling method), medium big to rather big areas (the statistical-dynamical downscaling method) or to the site (the spectral correction method).

Satisfactory results have been obtained in not-too-complex land terrains. There are however difficulties for very complex terrains, coastal and offshore conditions, not due to the concept of the methodologies themselves but due to the technical difficulties including (i) the limitations in the existing tools, e.g. the linear model LINCOM (ii) whereas it is relatively simple "terrain" offshore, models tend to oversimplify the situation. Complex dynamics, e.g. the air-sea interaction offshore conditions, has not been able to be taken into account in most modeling system.

To improve the situations in very complex land terrains, other microscale models than the linear model need to be investigated. To obtain improved estimations in the coastal and open water areas, the dynamics of waves and winds will have to be coupled in the modeling system.

13 Publications

- Larsén X.G., Badger J., Hahmann A. and Niels Mortensen (2012a): The selective dynamical downscaling method for extreme wind atlases. Wind Energy, in press.
- Larsén X.G., Ott S., Badger J., Hahmann A. and Mann J (2012b): Recipes for correcting the impact of effective mesoscale resolution on the estimation of extreme winds. Journal of applied meteorology and climatology, published, DOI 10.1175/JAMC-D-11.090.1.
- Larsén X.G., Mann J., Jørgensen H. and Rathmann O. (2012c): Uncertainties in using general extreme wind distribution and general pareto distribution for short time series. Manuscript in preparation. To be submitted to Wind Engineering or Nature Hazard.
- Badger J. and Larsén X.G. (2012): Application of reanalysis datasets for calculating extreme wind climate. Conference abstract attached. The 4th WCRP International Conference on Reanalysis, 7-11 May 2012, Silver Spring, Maryland USA.
- Larsén X.G., Badger J., Hahmann A. and Ott S. (2011a): Extreme wind atlases from the selective dynamical mesoscale modelling.

  *In Scientific Proceedings in European Wind Energy Annual Events March 2011, p186 - 189, Brussels.

  *Poster at the 12th WRF users' workshop in Boulder, Colorado, USA, June 2011.
- Larsén X.G., Ott S., Badger J., Hahmann A., Mann J. and Clausen N.E. (2011b): A recipe for correcting the effect of mesoscale resolution on the estimation of extreme winds. In Scientific Proceedings in European Wind Energy Annual Events March 2011, p213 - 216, Brussels
- Badger, Jake; Hahmann, Andrea N.; Larsén, Xiaoli Guo; Pena Diaz, Alfredo; Batchvarova, Ekaterina; Gryning, Sven-Erik; Floors, Rogier; Ejsing Jørgensen, Hans (2011c): Comprehensive utilization of mesoscale modelling for wind energy applications. Presented at: EWEA Annual Event 2011. Brussels (BE), 14-17 Mar, 2011 In: Proceedings : EWEA, 2011 (6 pages)
- Larsén X.G. and Mann J. (2011e): Extreme winds and turbulence at Østerild. Internal Report for Evaluation of the Østerild testing center.
- Badger J., Larsén X.G., Mortensen N.G., Hahmann A., Carsten J.C. and Jørgensen H. (2010): A universal mesoscale to microscale modeling interface tool. Full conference paper published in proceedings in European Wind Energy Conference and Exhibition 2010, 20-23 April, Warsaw, Poland, 6 pages.

Acknowledgement Thanks for the contributions from our colleagues from DTU Wind Energy, especially Andrea N. Hahmann for her expertise in mesoscale modeling, Niels G. Mortensen for the measurements from Gulf of Suez and for sharing his knowledge of using WAsP in complex terrains and Søren Ott for his sharp criticisms. Thanks also for the help from Javier Sanz, Elena Cantero and Christos Stathopoulos from CENER, Spain, with the studies in complex terrains. We acknowledge DONG Energy for the measurements from Horns Rev and Nysted through the PSO project "Mesoscale Variability". We are grateful for several other projects for sharing data with us, including Norsewind and Safewind.

References

[1] X.G. Larsén, J. Badger, A. N. Hahmann, and N. G. Mortensen. The selective dynamical downscaling method for extreme wind atlases. *Wind Energy, In press*, 2012.

[2] X.G. Larsén, S. Ott, J. Badger, A. Hahmann, and J. Mann. Recipes for correcting the effect of mesoscale resolution on the estimation of extreme winds. *J. Appl. Meteor. Climatol.*, 51:521 – 533, 2012.

[3] X.G. Larsén, J. Mann, H. Jørgensen, and O. Rathmann. Uncertainties of the return wind from short time series using general extreme wind distribution and general pareto distribution. *To be submitted*, 2012.

[4] J. Badger, X. G. Larsén, N.G. Mortensen, A. Hahmann, J.C. Hensen, and H. Jørgensen. A universal mesoscale to microscale modelling interface tool. European Wind Energy Conference, Warsaw, Poland, 20 - 23 April, 6 pages. 2010.

[5] J. Gross, A. Heckert, J. Lechner, and E. Simiu. Novel extreme value estimation procedures: Application to extreme wind data. In J. Galambos, J. Lechner, and E. Simiu, editors, *Extreme Value Theory and Applications*. Kluwer, Boston, 1994.

[6] J.P. Palutikof, B.B. Brabson, D.H. Lister, and S.T. Adcock. A review of methods to calculate extreme wind speeds. *Meteorological Applications*, 6:119–132, 1999.

[7] S. H. Seong. Parametric study based on synthetic realizations of EARPG(1)/UPS for simulation of extreme value statistics. *Wind and Structure*, 2:85–94, 1989.

[8] E. Kalnay, M. Kanamitsu, R. Kistler, W. Collins, D. Deaven, L. Gandin, M. Iredell, S. Saha, G. White, J. Woollen, Y. Zhu, M. Celliah, W. Ebisuzaki, W. Higgins, J. Janowiak, K.C. Mo, C. Ropelewski, J. Wang, A. Leetmaa, R. Reynolds, R. Jenne, and

D. Joseph. The NCEP/NCAR 40-year reanalysis project. *Bull. Am. Meteorol. Soc.*, 77:437–471, 1996.

[9] H.P. Frank. Extreme winds over Denmark from the NCEP/NCAR reanalysis. Technical Report Risoe-R-1238(EN), Risø National Laboratory, Roskilde, Denmark, *http://www.risoe.dk/rispubl/VEA/ris-r-1238.htm*, 2001.

[10] X.G. Larsén and J. Mann. Extreme winds from the NCEP/NCAR reanalysis data. *Wind Energy, DOI: 10.1002/we.318*, 12:556–573, 2009.

[11] X.G. Larsén, J. Mann, H. Göttel, and D. Jacob. Wind climate and extreme winds from the regional climate model REMO. In: Scientific Proceedings (on line). European Wind Energy Conference and Exhibition, Brussels, 31 March - 3 April, pages 58–62. 2008.

[12] X.G. Larsén and J. Mann. The effects of disjunct sampling and averaging time on mean maximum wind. *J. Wind Eng. Ind. Aerodyn*, 94:581–602, 2006.

[13] H. Tennekes. Similarity relations, scaling laws and spectral dynamics. In F. T. M. Nieuwstadt and H. van Dop, editors, *Atmospheric turbulence and air pollution modelling*, chapter 2, pages 37–68. D. Reidel publishing company, Dordrecht, 1982.

[14] R. Weisse, H.V. Storch, and F. Feser. Northeast Atlantic and North Sea storminess as simulated by a regional climate model during 1958-2001 and comparisons with observations. *Journal of Climate*, 18:465–479, 2005.

[15] J. Winterfeldt. Comparison of measured and simulated wind speed data in the North Atlantic. Technical Report PhD-Thesis, ISBN 0344-9629, GKSS-Forschungszentrum Geesthacht GmbH, GKSS Library, Postfach 11 60, D-21494 Geesthacht, Germany, 2008.

[16] N.W. Nielsen and B.H. Sass. A numerical, high resolution study of the life cycle of the severe storm over Denmark on 3 December 1999. *Tellus*, 55:338–351, 2003.

[17] S.C. Pryor, R.J.Barthelmie, N.E. Clausen, M. Drews, N. Mackeller, and E. Kjellström. Analysis of possible changes in intense and extreme wind speeds over northern europe under climate change scenarios. *Clim. Dyn.*, 2010.

[18] T. Hofherr and M. Kunz. Extreme wind climatology of winter storms in Germany. *Clim. Res.*, 41:105–123, 2010.

[19] M. Kunz, S. Mohr, M. Rauthe, R. Lux, and Ch. Kottmeier. Assessment of extreme wind speeds from Regional Climate Models - Part 1: Estimation of return values and their evaluation. *Nat. Hazards Earth Syst. Sci.*, 10:907–922, 2010.

[20] N.-E. Clausen, X.G. Larsén, S. Payor, and M. Drews. Chap. 7 wind power. In *Climate Change and Energy System, ISBN 978-92-893-2190-7*. 2011.

[21] Kanamitsu M., Ebisuzaki W., Woollen J., Yang S.-K., Hnilo J. J., Fiorino M., and Potter G. L. Ncep-doe amip-ii reanalysis (r-2). *Bull. Am. Meteorol. Soc.*, pages 1631–1643, 2002.

[22] O.B. Christensen, M. Drews, J.H. Christensen, K. Dethloff, K. Ketelsen, I. Hebestadt, and A. Rinke. The HIRHAM regional climate model version 5(β). In *Available online: http://www.dmi.dk/dmi/index/viden/dmi-publikationer/tekniskerapporter.htm*. 2006.

[23] J. Sanz and E. Cantero. Determination of vref using meteorological model outputs. *Euro FP7 Safewind project meeting, Fredericia Denmark, Feb. 2012*, 2012.

[24] P. A. Jimenez, J. F. González-Rouco, J. P. Montávez, J. Navarro, E. García-Bustamante, and F. Valero. Surface wind regionalization in complex terrain. *J. Appl. Meteorol. Clima.*, 47:308–324, 2008.

[25] P. Astrup, N. O. Jensen, and T. Mikkelsen. Surface roughness model for LINCOM. Technical Report Risø-R-900, Risø National Laboratory, Roskilde, Denmark, *URL:www.risoe.dk*, 1996.

[26] P. Astrup and S. E. Larsen. WAsP Engineering flow model for wind wind over land and sea. Technical Report Risø-R-1107, Risø National Laboratory, Roskilde, Denmark, *URL:www.risoe.dk*, 1999.

[27] L. Landberg, L. Myllerup, O. Rathmann, E.L. Petersen, B.H. Jørgensen, J. Badger, and N.G. Mortensen. Wind resource estimation - An overview. *Wind Energy*, 6:261–271, 2003.

[28] F. Frey-Buness, D. Heimann, and R. Sausen. A Statistical-Dynamical Downscaling Procedure for Global Climate Simulations. *Theor. Appl. Climatol.*, 50:117–131, 1995.

[29] G. Adrian and F. Fiedler. Simulation of unstationary wind and temperature fields over complex terrain and comparison with observations. *Beitr. Phys. Atmosph.*, 64:27–48, 1991.

[30] G. Adrian. Zur dynamik des windfeldes uber orographisch gegliedertem gelnde. *Ber.a Deutscher Wetterdienst*, 188, 1994.

[31] Joseph B. Klemp and Dale R. Durran. An upper boundary condition permitting internal gravity wave radiation in numerical mesoscale models. *Monthly Weather Review*, 111(3):430–444, 1983.

[32] K.S. Gage and G.D. Nastrom. Theoretical interpretation of atmospheric wavenumber spectra of wind and temperature observed by commercial aircraft during GASP. *J. Atmos. Sci.*, 43:729–740, 1986.

[33] E. Lindborg. Can the atmospheric kinetic energy spectrum be explained by two-dimensional turbulence? *J. Fluid Mech.*, 388:259–288, 1999.

[34] X.G. Larsén, C. Vincent, and S. Larsen. The spectral structure of mesoscale winds over water. *Q. J. R. Meteorol. Soc., In press*, 2012.

[35] C. Stathopoulos, N. Barranger, X. G. Larsén, and J. S. Rodringo. Implementation of spectrum analysis in mesoscale modeling for wind energy assessment studies. *12th EMA/ 9th ECAC Annual Meeting Abstracts*, 9:EMS2012–282, 2012.

[36] J. Mann, L. Kristensen, and N. O. Jensen. Uncertainties of extreme winds, spectra and coherences. In Larsen and Esdahl, editors, *Bridge Aerodynamics, ISBN 9054109610*. Rotterdam, Balkema, 1998.

[37] P. A. Jimenez, J. F. González-Rouco, E. García-Bustamante, J. Navarro, J. P. Montávez, J. Vilà-Guerau De Arellano, J. Dudhia, and A. Muñoz-Roldan. Surface wind regionalization over complex terrain: Evaluation and analysis of a high-resolution wrf simulation. *J. Appl. Meteorol. Clima.*, 49:268–287, 2010.

[38] S. Reid and R. Turner. Correlation of real and model wind speeds in different terrains. *Wea. Forecasting*, 16:620–627, 2001.

[39] J. Abild. Application of the wind atlas method to extremes of wind climatology. Technical Report Risoe-R-722(EN), Risø National Laboratory, Roskilde, Denmark, 1994.

DTU Vindenergi er et institut under Danmarks Tekniske Universitet med en unik integration af forskning, uddannelse, innovation og offentlige/private konsulentopgaver inden for vindenergi. Vores aktiviteter bidrager til nye muligheder og teknologier inden for udnyttelse af vindenergi, både globalt og nationalt. Forskningen har fokus på specifikke tekniske og videnskabelige områder, der er centrale for udvikling, innovation og brug af vindenergi, og som danner grundlaget for højt kvalificerede uddannelser på universitetet.

Vi har mere end 240 ansatte og heraf er ca. 60 ph.d. studerende. Forskningen tager udgangspunkt i ni forskningsprogrammer, der er organiseret i tre hovedgrupper: vindenergisystemer, vindmølleteknologi og grundlag for vindenergi.

Danmarks Tekniske Universitet
DTU Vindenergi
Nils Koppels Allé
Bygning 403
2800 Kgs. Lyngby
Telefon 45 25 25 25

info@vindenergi.dtu.dk
www.vindenergi.dtu.dk